COMOTI
ROMANIAN RESEARCH & DEVELOPMENT INSTITUTE FOR GAS TURBINES

TURBO

Scientific Journal

vol. VI (2019), no. 2

COMOTI
ROMANIAN RESEARCH & DEVELOPMENT INSTITUTE FOR GAS TURBINES

DEFENSE INDUSTRY

We power Navy

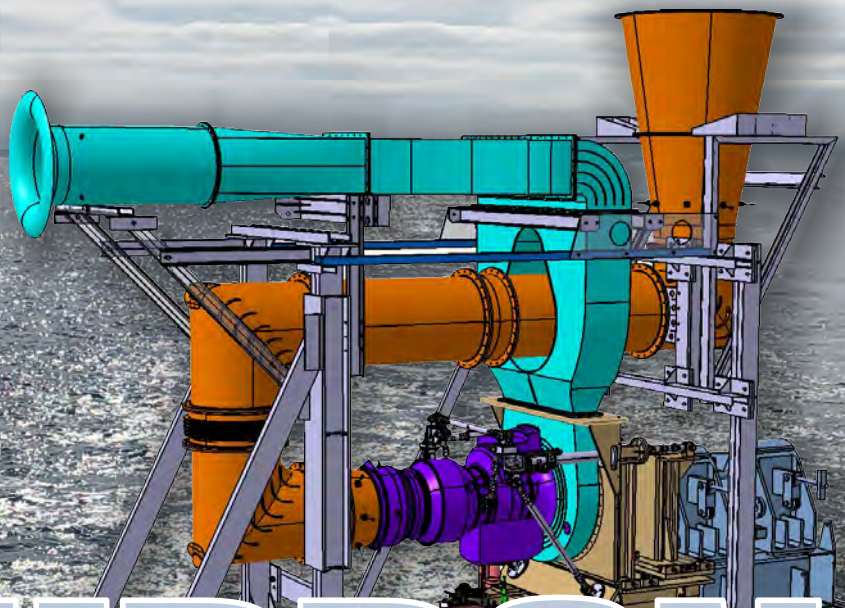

TURBONAV

- Turbine of the T22 frigates aggregate repairs;
- Technical inspection of the propulsion system of the T22 frigate;
- Revision and expertise of propulsion systems of Romanian Military Navy ships to extend service life;
- Research by bench testing of marine propulsion engines.

COMOTI powers NAVY

EDITORIAL

Identificarea nevoii societale (1)

Fie că este vorba de ştiinţă sau de politică, Max Weber viza acelaşi scop: să extragă etica specifică unei activităţi pe care o dorea conformă cu finalitatea sa

Raymond ARON

Viața oricărei persoane moderne este asociată, mai mult sau mai puțin conștient, așteptării societale. Putem spune că suntem imersați în așteptare, că depindem de ea și o influențăm. Cumpărăm mărfuri din magazine mici ori hipermarketuri, ne instruim în școli și universități, folosim produse realizate în fabrici, avem relații cu băncile.

Ca o concluzie, suntem angajați ai unor instituții/organizații și clienți ai altora. Toate aceste lucruri determină o creștere mai mare ca niciodată a valorii organizațiilor și a activităților organizaționale.

Teoria organizației este o știință bine formată, fondator al acestei discipline fiind considerat sociologul, avocatul, economistul și istoricului german Max Weber (1864-1920) cel care a trasat așa-numita direcție birocratică în dezvoltarea teoriei managementului și organizării.

În scrierile sale despre raționalizarea societății, căutând un răspuns la întrebarea ce trebuie făcut pentru ca întreaga organizație să funcționeze ca o mașină, acesta a subliniat că ordinea, susținută de reguli relevante, este cea mai eficientă metodă de lucru pentru orice grup organizat de oameni.

El a considerat că organizația poate fi descompusă în părțile componente și se poate normaliza activitatea fiecăreia dintre aceste părți, a propus astfel să se reglementeze cu precizie numărul și funcțiile angajaților și ale organizațiilor, a subliniat că organizația trebuie administrată pe o bază rațională/impersonală. În acest punct, aspectul social al organizației este foarte important, oamenii fiind recunoscuți pentru ideile, caracterul, relațiile, cultura și deloc de neglijat, așteptările lor. Astăzi, aparenta omnipotentă a civilizației noastre este plină de amenințări la adresa umanității și a întregii vieți pe Pământ, inclusiv amenințarea continuă a unui război nuclear global și a tulburărilor geochimice și climatice sistemice, în echilibrul planetei.

Dezvoltarea rapidă a tehnologiilor digitale și materiale precum și noile instrumente de management din secolul XXI oferă omenirii oportunități fără precedent de a crea un viitor optimist la scară globală. În întreaga istorie a Pământului nu au existat astfel de circumstanțe pentru a influența mediul: s-au creat mijloace de protejare față de efectele ostile ale climatului și agenților patogeni, s-au creat sisteme globale de aprovizionare cu alimente, există metode de influență genetică și s-au accelerat cercetări care ne pot transforma într-o specie cosmică ce trăiește pe mai multe planete.

La începutul secolului XX în lume au trăit puțin mai mult de un miliard și jumătate de oameni, în 100 de ani ne-am înmulțit la șapte miliarde și jumătate iar specia noastră continuă să trăiască după tipare și norme culturale dezvoltate atunci când oamenii erau mult mai puțini. În același timp și cumva în mod paralel, creația civilizației noastre – tehnosfera, devine rapid autonomă, inteligentă și uneori chiar greu accesibilă propriei noastre înțelegeri.

Organizațiile publice sunt create pentru a răspunde nevoilor și intereselor sociale ale oamenilor, iar eficacitatea organizației depinde de potențialul de resurse al acesteia și de interacțiunea sistemică a acestora, luând în calcul echipamentele de producție, potențialul intelectual și puterea de muncă a angajaților, resursele financiare sau imaginea companiei.

În stuctura industrială actuală, aproximativ jumătate dintre ocupații conțin elemente de rutină, fie că este vorba de muncă fizică sau muncă intelectuală, inclusiv marketing, finanțe, comunicații etc. Pe termen lung însă, aceste ocupații pot fi înlocuite cu inteligență artificială sau roboți. Mai mult, unele tehnologii, cum ar fi nano - sau biotehnologie, pot duce la o revoluție a întregii industrii și la apariția rețelelor de producție regenerative.

EDITORIAL

Identificarea nevoii societale (2)

Sectoare de tehnologie noi vor apărea ca urmare a dezvoltării unei noi generații de tehnologii de uz industrial și de consum, precum dezvoltarea și programarea sistemelor energetice și a altor medii inteligente pentru localități și gospodării, sau producția de roboți urbani și vehicule autonome fără pilot, precum și dezvoltarea și producerea de materiale de bioinginerie regenerabile.

Există însă două însușiri ale omului care sunt imposibil de imitat: creativitatea și umanitatea. De aceea un număr foarte mare de activități pe care oamenii le pot oferi în educație, sănătate, artă, design sau chiar divertisment, vor rămâne subordonate acestor două însușiri.

Prin prisma acestor însușiri educația poate oferi mult mai mult decât instruirea în abilitățile necesare socializării ca simplu angajat și cetățean. Poate ajuta la restabilirea sensului vieții și la furnizarea ocaziei fiecăruia de a face lucruri care îl inspiră.

Economiile virtuale, create în mediul online, de la jocuri la rețele sociale, în care oamenii pot găsi un număr imens de activități, de la simulări de proiectare ori simulări numerice, deoarece realitatea virtuală permite depășirea aproape oricăror restricții care există în realitatea materială, crează lumi cu reguli ce par imposibile sau puțin probabil să fie reale.

O economie verde care își propune nu numai crearea de procese și produse durabile, în conformitate cu reglementările ONU, profesii ecologice și metode de restabilire a echilibrului dintre umanitate și planetă, în care tot mai mulți oameni au rolul de a ajuta la protejarea și dezvoltarea ecosistemului global natural, prin utilizarea pe scară largă a soluțiilor automate, cum ar fi robotica, internetul și inteligența artificială, dezvoltarea imprimării 3D și a altor tehnologii aditive, precum și prin utilizarea pe scară largă a bio - producției ecosistemice de produse alimentare, energiei și materialelor, posedă uriașul potențial de a dezvolta civilizația la nivelul abundenței totale.

Răspândirea inovației tehnologice continuă să aibă un impact major asupra societății, organizațiilor și comunităților. Accelerarea schimbării este însoțită de creșterea fluidității mediilor sociale care sunt din ce în ce mai influențate de variabilitatea socială, politică și economică, de incertitudine și de complexitate.

Într-o situație de creștere exponențială a datelor și a cunoștințelor științifice, inteligența artificială poate juca un rol în integrarea cunoștințelor și în susținerea luării deciziilor colective, iar principalul obstacol în calea evoluției sociale poate fi capacitatea noastră colectivă de a crea și susține noi dezvoltări, crearea de cunoștințe și managementul ecosistemelor capabile să facă față complexității societale crescânde.

Tranziția la o societate bazată pe principiile durabilității va trebui să țină cont de preferințele, interesele și alegerile colective, limitările și prejudecățile cognitive, dar și de cunoștințele, competențele, practicile, tehnologiile pe care le inițiem și dezvoltam și care pot fi motiv pentru desfășurarea crizei existențiale.

Modele de sisteme sociale, create în era de relativă stabilitate a trecutului, par să nu fie potrivite pentru viitor. Apariția unui nou sistem financiar, inclusiv criptomonede și alte sisteme de gestionare a averii, dar și modificările valorilor și motivației emoționale, fără a se pune accent pe acumulare și pe bani, oferă o șansă de a recunoaște valoarea de unicitate a omului, cu înțelepciunea, grija, compasiunea și dragostea la scară globală.

Autor: ec. Elena Banea

Decembrie 2019

EDITORIAL

Identification of Societal Needs (1)

Whether science or politics were in question, Max Weber had in mind a single purpose: to extract the ethics specific to a certain activity so that it would answer its very scope.

Raymond ARON

Life of any modern person is more or less consciously associated with societal expectation. We may say that we are plunged into expectation, that we depend on and influence it at the same time. We purchase goods from shops and hypermarkets, we instruct ourselves in schools and universities, we use products developed in plants, and we collaborate with banks. Ultimately, we are either employees of some institutions/organizations or the clients of others. All these things determine an ever larger growth than ever of the value of organizations, as well as of the organizational activities.

The theory of management is a well grounded science, the founder of this discipline being considered to be Max Weber (1864-1920), a German sociologist, lawyer, economist and historian, the one who introduced the so-called birocratic direction as part of the development of the theory of management and organization.

In his writings on the rationalization of society, while searching for an answer to the question about what was to be done so that *the entire organisation may work as a machine*, he underlined that order, supported by relevant rules, is the most efficient working method for any organized group of people. He considered that any organization can be *decomposed* into its component parts and that the activity of each of these parts can be *structured*; therefore, he proposed a strict limitation of the number and positions of the employees and compartments, and he insisted on the fact that the organization must be managed on a rational/objective basis. At this point, the social aspect of the organization is extremely important, people being appreciated for their personal ideas, character, relationships, education and, last but not least, for their own expectations.

Nowadays, the apparent omnipotency of our civilisation is full of threats to humanity and to the whole life on Earth, including the permanent threat of a global nuclear war, as well as of systemic geochemical and climate changes in the ballance of the planet.

Fast development of digital and material technologies, as well as the new 21st century management tools provide humanity with unprecedented opportunities to develop an optimistic future for society at large. The whole history of the Earth hasn't ever recorded any similar circumstances that may have an impact on the environment: new means of protection against hostile climate effects and patogenic agents have been generated, global systems of food supply have been developed, methods of genetic influence are also existent, and accelerated research has been made on mankind's possibility of becoming a cosmic species that might live on other planets.

At the beginning of the 20th century, a little over a billion and a half people lived on earth; one hundred years later, the overall population reaches seven billion and a half, while our species goes on living on cultural patterns and norms that were developed in times when the number of people was significantly smaller. At the same time, and somehow independently, the very creation of our civilization – the techno sphere, tends to become autonomous, intelligent, and, in certain cases, even hardly accessible to our own understanding.

Public organizations are set up to answer the social needs and interests of the individuals, and the efficiency of any organization depends on its resource potential, as well as on the systemic interaction of those resources, if we refer to production equipment, to the intellectual potential and the working power of its employees, but it also depends on the financial resources and the visibility of the company.

Almost half of the jobs included in the present industrial structure contain some *routine* elements, whether we refer to physical or intellectual work, including marketing, finances, communications, etc. In the long run, though, these jobs may be replaced by artificial intelligence or robots.

EDITORIAL

Identification of Societal Needs (2)

Furthermore, some technologies, nano for example – or the bio technology, may lead towards a complete industrial revolution and to the emergence of regenerative production networks. New technology areas will come out as a consequence of the development of a new generation of industrial and domestic technologies, such as the development and programming of energy systems and of other intelligent environments destined for open places and households or the production of urban robots and of autonomous vehicles, but also the development and production of regenerating bio engineering materials.

Still, there are two human features that cannot be reproduced at all: creativity and humanity. That is why a very large number of activities, which men are able to supply in domains like education, health, arts, design or even entertainment, will always depend on these two features. Considering these two above mentioned features, we may say that education can offer much more than a simple training of social abilities of any employee or citizen. It can lead to redefining the sense of life, but also to facilitating anyone the occasion to do things that may inspire her/him.

Virtual economies created online, be them games or social networks, where people can discover an endless number of activities, such as, for example, design or numeric simulations, due to the fact that virtual reality allows transcendence of almost any restriction existent in actual reality, but it also sets up distinct environments with rules which seem impossible or highly improbable to be real.

Any friendly economy, which takes into consideration not only the development of durable processes and products, according to the UNO regulations, *ecological professions* and methods of ballance resetting between humanity and the earth, in which more and more people get involved to help to protect and develop the natural global ecosystem by a large scale use of automatic solutions, such as robotics, the Internet and artificial intelligence, through the development of 3D imprinting and of other additive technologies, as well as by a large scale use of ecosystemic bio-production of food supplies, energy and materials, has the huge potential of providing the development of our civilization towards overall abundance.

Dissipation of technological innovation still has a major impact on society, organizations and communities. The acceleration of change is accompanied by extension of social media fluidity, which are more and more clearly influenced by social, political and economic changes, as well as by incertitude and complexity.

Given a specific exponential raise in scientific data and knowledge, artificial intelligence may play a certain role in data integration and support of collective decision taking, while the main obstacle against social evolution may reside in our collective capacity to design and support new developments, knowledge advance and the management of ecosystems capable of coping with the ever growing societal complexity.

Transition towards a society based on durability principles will have to consider collective preferences, interests and choices, cognitive limitations and prejudices, but also it will have to respond to the knowledge, competences, practices and technologies that we innitiate and develop, and that may all stand for further extention of the existential crisis.

Various models of social systems set up during relatively stable past years do not seem to be appropriate in the future. The emmergence of a new financial system, cripto coins included, as well as of other systems of wealth management, and also the changes in value and emotional motivation, without any specific insistance on accumulation and money, facilitates the recognition of man's unique value, as far as his wisdom, care, compassion and love are concerned anywhere on earth.

Author: ec. Elena Banea

December 2019

More information regarding the scientific journal can be found at:
http://www.comoti.ro/ro/jurnalul_stiintific_turbo.html
turbojournal@comoti.ro
jeni.popescu@comoti.ro

ISSN: 2559-608X
ISSN-L: 1454-2897
Scientific Journal TURBO is included in ICI World of Journals:
https://journals.indexcopernicus.com/search/details?id=48512
ICV 2017: 63,88

CONTENTS

HARDWARE IN THE LOOP TEST PLATFORM CONCEPT FOR ADAPTIVE TURBINE ENGINE CONTROLLER

Adrian STOICESCU[1,2], Razvan CIOBANU[1], Alexandra ȚĂRANU[1,2], Cristian NECHIFOR[1,2], Filip NICULESCU[1,2]

ABSTRACT: Hardware in the loop simulation has gained much attention during the last years in both research and engineering areas. It allows testing embedded controllers using simulation models of the controlled plant, such as a real engine. The challenges are making an adequate simulation platform so that the testing scenarios for the developed controller will be as close as possible as with a real engine. This paper presents a dedicated Hardware in the loop test platform concept for an innovative turbine engine controller. This way, its development and testing time and costs are minimized, while as much simulation accuracy is brought into the testing procedure. The controller is a neural network-based adaptive ECU that aims at bringing major improvements to the engine control efficiency. Based on preliminary analysis, the proposed HIL platform is described as a concept, is technically achievable and expected to become a prototype within future work.

KEYWORDS: Hardware in the Loop, Simulation, Turbine Engine, Controller, ECU

NOMENCLATURE

ADC – Analog Digital Converter
AI – Analog Input
ANN – Artificial Neural Network(s)
CLOCK – Internal ECU Clock
COM UART – UART Protocol Programming Interface
CPU – Central Processing Unit
DAC – Digital Analog Converter
DC – Direct Current
DEMUX - Demultiplexer
ECU – Engine Control Unit
EHCV – Electrohydraulic Check Valve
FPGA – Field Programmable Gate Array
HIL – Hardware in the loop
I/O – Input/Output
kS – kyloSamples
OS – Operating System
PCB – Printed Circuit Board
PHT2 – Turboshaft engine
SS – State Space
SG – Starter Generator
TF – Transfer Function
WD – Watch Dog
β_{TL} – Throttle Lever Control Input
δEHCV FI – Electrohydraulic Check Valve for Fuel Injector Control Circuit
δEHCV FS – Electrohydraulic Check Valve for Fuel Supply Control Circuit
δFP – Fuel Pump Power Control Circuit
δIGP – Injector Glow Plug Power Control Circuit

[1] Romanian Research and Development Institute for Gas Turbines COMOTI, Bucharest, Romania
[2] University Politehnica of Bucharest, Romania

δSG Mode – Starter Generator Mode Selector
χEGT – Exhaust Gas Temperature Input
χNCC – Centrifugal Clutch Speed Input
χNGT – Gas Turbine Speed Input
χTAT – True Air Temperature Input

1. INTRODUCTION

Hardware in the loop (HIL) platforms are increasingly used during development and testing stages of control systems. The plant under control, such as a turbine engine, is simulated by using mathematical models in a virtual environment on a dedicated hardware platform. The simulation interacts continuously with the controller, as if it were the real plant. This allows for developing new hardware and software solutions within time and quality restrictions imposed by markets. Turbine engines are costly machines. Using HIL platforms when developing and testing ECU (Engine Control Unit) controllers provide the means for performing a wide range of scenarios while the engine is either not physically available or risky enough to use it. An automotive ECU HIL system is described in [1]. In [2], the authors developed a HIL simulation platform for testing a jet engine fuel controller. The engine model shown in [2] is based on two parts: a nonlinear equation system describing thermodynamic relations in the compressor, turbine and nozzle, and dynamic nonlinear equations describing the transcient process. A HIL simulation for turbofan engine is described in [3]. This paper proposes a HIL test platform concept for an adaptive turbine engine ECU which undergoes design phase.

ECUs are fundamentally important in determining fuel flow, as well as the logic dealing with engine's constraints. These controllers need to be adapted based on the engine performance characteristics. The most widely used control strategy for turbine engines is Min-Max [4]. This is based on selecting, at any moment, one of multiple engine control loops, such as: steady-state control loop, acceleration/deceleration control loops, critical situations, etc. Intelligent control strategies have gained attention among researchers, in order to increase the performance and flexibility of the controller. In [5], a combination of fuzzy logic and evolutionary algorithms was studied with the aim towards a gas turbine aero-engine. Other studies regarding fuzzy logic and artificial neural networks (ANN) have been conducted and shown in various papers [6-8]. However, most of them have not exceed research stages. The HIL test platform proposed in this paper is a concept adapted for testing an ANN-based controller which is undergoing the design stage.

2. CONTROLLER OPERATION ANALYSIS

The adaptive turbine engine controller is an ECU (Engine Control Unit) designed for a particular type of miniature single-shaft turbine engine. As an innovative controller, the ECU logic is made so that the output is based not on predefined logic, but determined based on adaptive algorithms. The controller is based on a ECU-type embedded hardware module that includes a PCB, with the main component blocks shown in Fig. 1, and software routines. Parts of the routines will be enhanced with blocks for generating fuel flow signal output based on ANNs, previously trained on gathered data sets and simulations. Generally, international approaches on similar topics lead to a fuzzy logic or multilayer feed-forward neural network, which is also the basis for the ECU under development. However, to the authors' knowledge, their TRL only ranges from technology concept to experimental model.

For developing the ECU circuit diagram, it was necessary to identify the dynamic model of the equipment used to control the turbine engine and of the turbine engine itself. This was achieved with the use of system dynamics identification via experimental testing (Fig. 2). Equipment such as electrohydraulic check valves, fuel injector, glow plug, fuel pump and starter generator were tested at full operational limits. After the testing, the data was plotted in order to achieve graphical analysis (EHCV fuel dosage according to modulation frequency and pump supply voltage; glow plug temperature – supply voltage dependency) of the system, later on being used as input data for modelling transfer functions of the previously mentioned equipment. The ECU was designed with transient operational capability other than steady state operation wich does not require a nonlinear system modelling. As a result, continuous-time instead of discrete transfer functions were used.

After determining the polynomial coefficients of the transfer functions, the equipment dynamic model was developed and tested for step response. In order to mimic ECU control logic, conditioning blocks were also implemented (such as EGT Start Conditioner or Start Attempt Control Loop). For implementing operational control safety measures, interlocks were also introduced as primary backup conditioning loop in order to eliminate logic infringements.

After the controller undergoes HIL testing, it is expected to achieve improvements such as: reducing engine starting time and fuel consumption, decreasing signal overshot, decreasing energy losses during transient operation, as is described in previous research [9].

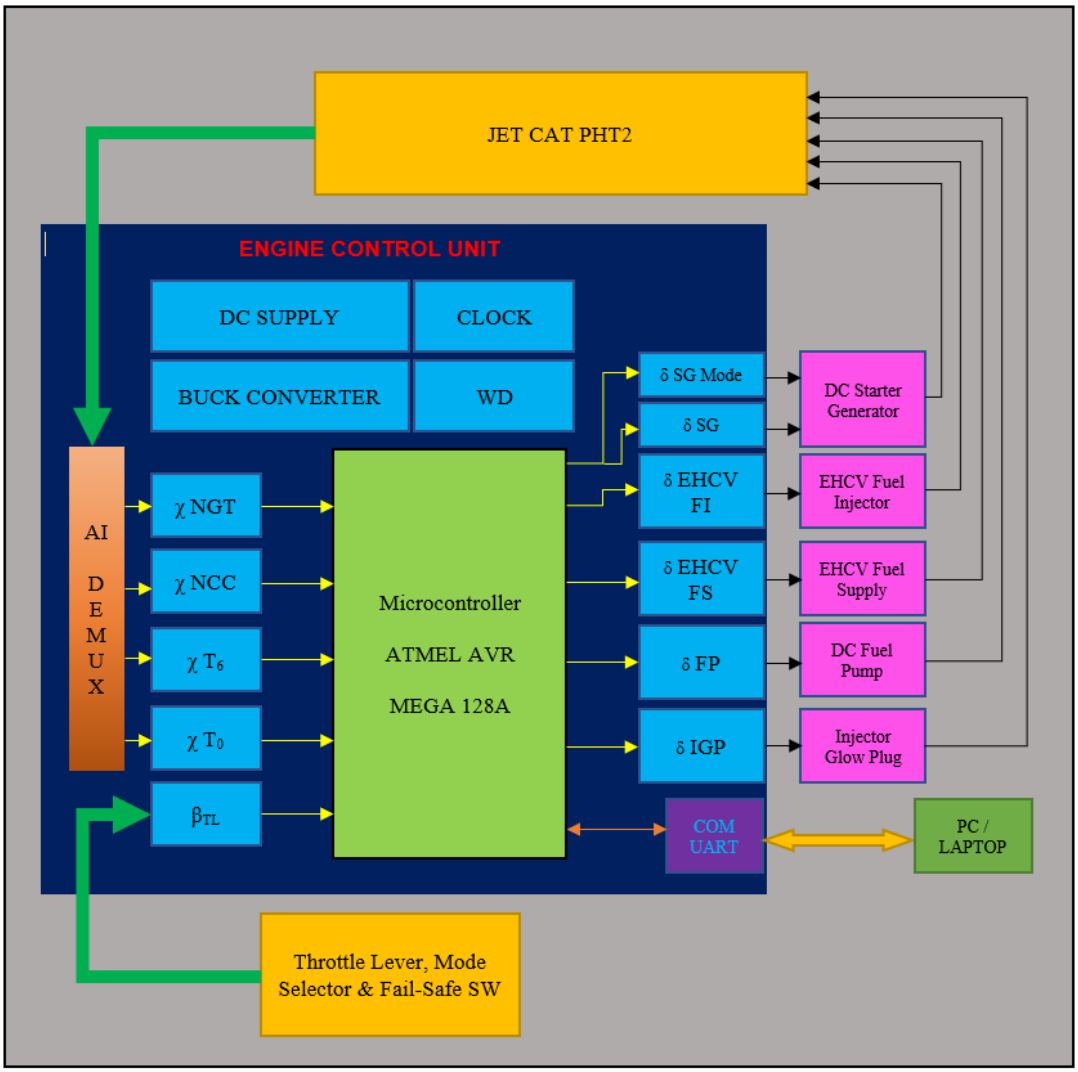

Fig. 1 ECU block diagram

Fig. 2 SG Test bench used for system model identification

3. HIL PLATFORM CONCEPT

The HIL platform suggested for this type of controller will basically have these main roles: a) simulation of the turbine engine the real ECU interacts with; b) electrical signal generation towards the ECU as if the model had real sensors; c) receive and process signals from the ECU to influence model operation accordingly; d) allow user to control the throttle control of the simulated engine; e) user interface, error management and data logging. This essentially acts as a closed-loop control system, where feedback is taken from the simulated engine, processed by the ECU, which then controls the engine simulation, as seen in Fig. 3.

There are several aspects to be considered when designing a proper HIL platform for a turbine engine. Most of them revolve around the fact that the HIL testing needs to perform real-time plant simulation. This requires that everything on the platform needs to be compatible with real-time computing: processor, operating system, runtime environment, control loop architectures, signal acquisition and processing frequency/bandwidth. The engine model needs to execute at the same rate as the actual physical engine and be accurate (complex) enough for the purpose of the simulation.

Another fact is how much of the engine subsystems (engine components, sensors, actuators, etc.) are simulated as software routines or provided as real subsystems connected to the platform. While real components would make the simulation more accurate, an accurate enough submodel for each subsystem would be more cost effective. This is true in terms of parts needed for implementation, long-term reliability, however the work to create each model needs to be taken into account.

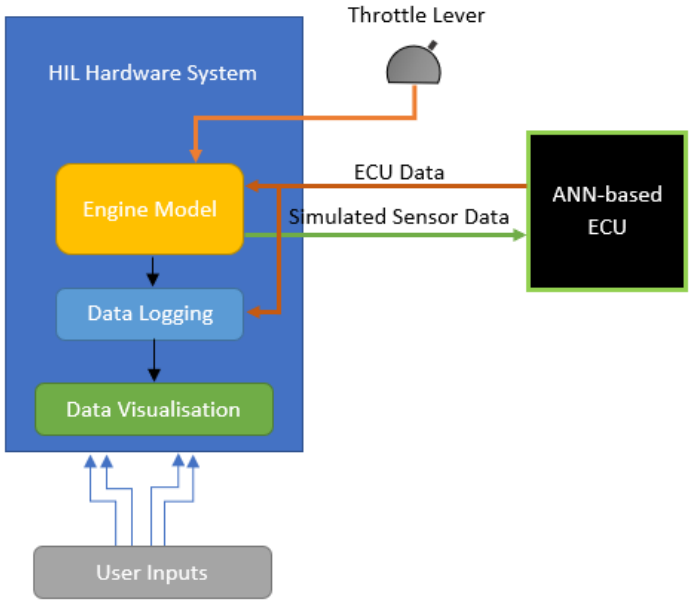

Fig. 3 HIL platform block and data flow diagram

The model

The engine chosen to be test subject for the HIL platform simulation is a miniature single-shaft turbine engine, consisting mainly of a turbine, a centrifugal clutch, a starter generator and a rotor shaft. In order to determine the dynamic model for this specific machinery, the real engine will be submitted to several operation stages. Based on determined performance map, transfer functions will be defined. The measurement setup includes: fuel pump control voltage, pump output fuel flow, combustion output valve flow, intake valve flow, igniter control voltage, injector temperature sensor, gas intake pressure and temperature sensors, compressor speed sensor, clutch speed sensor, starter generator control voltage.

The test rig is designed so that it can integrate and extend to a large variety of process instrumentation sensors and systems with the data acquisition setup. The data acquisition setup is based on an embedded controller featuring an FPGA and a real-time CPU running Linux Real-Time OS.

The dynamic model of the engine includes the following major subsystems: start sequencer, combustion chamber, starter stop and virtual instrumentation. The start sequencer subsystem models the starting sequence of the engine and its ignition elements, following a specific logic so that the ignition is successfully simulated. The combustion chamber subsystem models the gas dynamic and mechanical processes in the chamber. The starter stop subsystem models the cut off sequence when the conditions are met. The virtual instrumentation facilitates parameters visualization and control access to the simulation. A generic overview of the model architecture developed in Simulink is shown in Fig. 4.

The turbine engine's dynamic model is developed by simulating individual components rather than a whole SS black box type model (e.g. EHCV dynamic model, fuel Injector dynamic model, combustion chamber model).

HIL platform I/O

Starting from Fig. 3, we can deduce that, from a user perspective, the only main variable control towards the (simulated) engine, in the suggested architecture, is the throttle lever. An actual lever will be provided, as well as the possibility of manual control via software interface. Other controls are activation/deactivation of sequences, including engine simulation operation stages, (simulated) environment data input and auxiliary settings (data logging, signal range etc).

All engine instrumentation will be simulated and generated as real signals towards the ECU. Simulated sensor data towards the ECU include mainly the following output signals: Throttle Lever position, Igniter Check Valve 1/0, Igniter Check Valve Flow, Fuel Check Valve 1/0, Fuel Check Valve Flow, Gas Turbine Speed, Exhaust Gas Temperature, Starter Generator Speed, Starter Generator 1/0, Centrifugal Clutch Speed, Intake Gas Temperature, Atmospheric Pressure, True Air Temperature, Glow Plug 1/0, Fuel Injector Temperature, Fuel Pump 1/0, Fuel Pump Flow, Engine Mode 1/0 and Vibration.

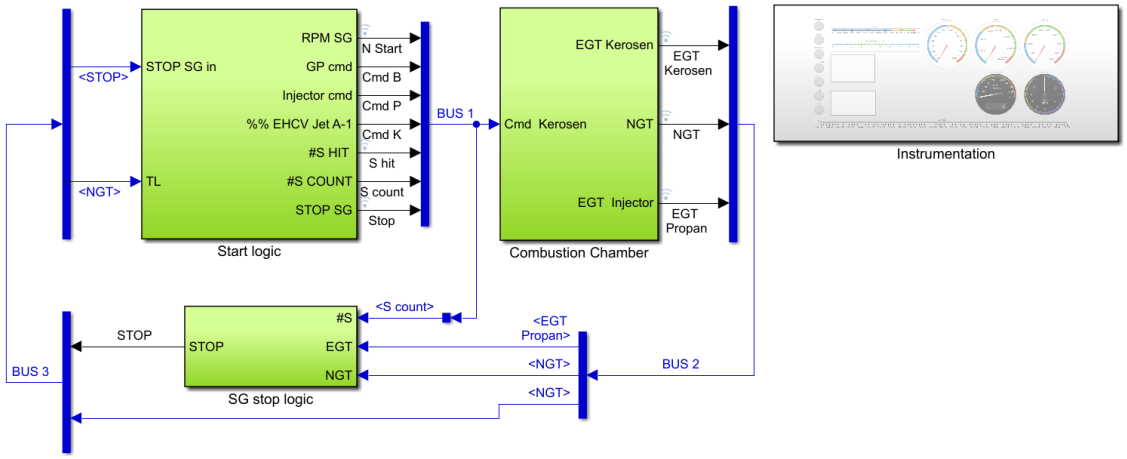

Fig. 4 Engine dynamic model – generic blocks overview

HIL platform architecture

The architecture revolves around a configuration, with an embedded controller similar to the previously mentioned data acquisition setup, featuring: a real-time 1.33 GHz dual-core CPU, 1 GB RAM memory, Linux Real-Time OS, an I/O chassis including a ±10 V 250 kS/s, 32-channel Analog Input voltage module, an 8-channel thermocouple input module, a 5V/TTL bidirectional I/O module and a ±10 V, 25 kS/s 16-channel Analog Output voltage module. The I/O modules configuration is designed to cover all signal types and number listed above, with the appropriate sample rate.

The VeriStand software will be used to run the simulation including the engine model developed in Simulink. This environment facilitates configuring I/O channels, data logging, stimulus generation for the ECU. VeriStand project files will be transferred to the Real-Time controller, while a remote computer will be permanently connected to it for user interface, logging, alarms and other such functions.

4. CHALLENGES AND FUTURE WORK

In this case, there are mainly two clearly defined systems operating in a loop: the specific control system (ECU) and the simulated engine system. For the HIL platform, a real-time embedded controller is chosen for the application, which is a low to medium sized hardware configuration controller. The configuration, in terms of both hardware resources and I/O specifications, is specifically designed for a) the type of ECU described earlier in this paper, and b) the model complexity. One of the main challenges regarding the implementation is the balance between the model complexity and hardware resources. The model needs to be accurate enough but not more complex than necessary for this specific purpose.

Future implementations of HIL platforms will include designing and configuring a more advanced HIL system. This is aimed at having a higher degree of integration with mathematical models and physical interfaces, in order to perform HIL testing of the highest level for a wider range of control systems. Building such a system will involve assembling and configuring all components for integration, testing and proper operation. Instrumentation and communication lines are also an important part. Several interfaces and interface modules and converters need to be properly implemented, while full compatibility and sustaining real-time frequency might prove to be a challenge. Software configuration includes routines such as: connection to the control system, running the model, data logging and interface.

Testing any of the HIL platforms will be made by simulating inputs, analysing outputs, evaluating time response, functionality and safety and submitting to specific scenarios. Optimization stages provide the means to address failures, inconsistencies, or other issues following testing stages.

5. CONCLUSION

A HIL platform is an undoubtedly useful tool that can significantly decrease time and consts of development and testing stages of embedded controllers. Due to the presented ECU technology being highly innovative and mostly studied as a state-of-the-art concept for engine control methods, to the authors' knowledge there is no reported HIL platform for ANN-based ECUs described in the scientific literature. While a real turbine engine can cost up to millions, a HIL simulation can mitigate all the risks related to worst case scenarios, due to engine failures being only simulated in this case. The concept was defined so that the ECU would not 'know' the difference between the simulator and the actual engine, with an emphasis on real electrical signals, data transfer frequency and an environment that allows for accurate engine models. The proposed HIL platform is promising, technically achievable and its development will be the basis for further extensions, in order to cover a wider application area of turbomachinery control system testing.

ACKNOWLEDGEMENT

This work was carried out within "Nucleu" Programs TURBO 2020+ and TURBOPROP, supported by the Romanian Minister of Research and Innovation, project numbers PN 18.10.01.04 and PN 19.05.01.01.

REFERENCES

[1] A. Cebi, L. Guvenc, M. Demirci, C. Karadeniz, K. Kanar, and E. Guraslan; 2005; "A Low Cost, Portable Engine Electronic Control Unit Hardware-in-the-Loop Test System"; *Proceedings of the IEEE International Symposium on Industrial Electronics*; Vol. 1; Dubrovnik, Croatia; June 20-23, 2005; pp. 293-298;
[2] M. Montazeri-Gh, M. Nasiri, S. Jafari; 2011; "Real-time multi-rate HIL simulation platform for evaluation of a jet engine fuel controller"; *Simulation Modelling Practice and Theory*; Vol. 19; Issue 3; pp. 996-1006;
[3] W. Bao, Y.F. Sui, Z.M. Liu, J.F. Liu; 2006; "Design and Realization of Hardware-in-the-loop Simulation for Turbofan engine"; *Journal of System Simulation*; Issue 6; pp. 1516-1519;
[4] S. Jafari, T. Nikolaidis; 2018; "Turbojet Engine Industrial Min-Max Controller Performance Improvement Using Fuzzy Norms"; *Electronics*; Vol. 7; Issue 11; pp. 314-327;
[5] A. J. Chipperfield, B. Bica, P. J. Fleming; 2002; Fuzzy scheduling control of a gas turbine aero-engine: a multiobjective approach; *IEEE Transactions on Industrial Electronics*; Vol. 49; No. 3; pp. 536-548;
[6] A. Zilouchian, M. Juliano, T. Healy, J. Davis; 2000; Design of a fuzzy logic controller for a jet engine fuel system; *Control Engineering Practice*, Vol. 8, No. 8, pp. 873–883;
[7] S. S. Tayarani-Bathaie, Z.N. Sadough Vanini, K. Khorasani; 2014; Dynamic neural network-based fault diagnosis of gas turbine engines; *Neurocomputing*; Vol. 125, pp. 153-165;
[8] R. Mohammadi, E. Naderi, K. Khorasani, S. Hashtrudi-Zad; 2010; Fault Diagnosis of Gas Turbine Engines by Using Dynamic Neural Networks; *ASME Turbo Expo 2010: Power for Land, Sea, and Air*; Vol. 3; Glasgow, UK; June 14-18, 2010;
[9] R. Ciobanu, A. Stoicescu, C. Nechifor, A. Taranu; 2018; Self-Learning Control System Concept for APU Test Cells; *MATEC Web of Conferences*; Vol. 210, 02009; 22nd International Conference on Circuits, Systems, Communications and Computers (CSCC); Majorca, Spain; July 14-17, 2018.

FT-IR SPECTROSCOPY USED FOR MINERAL COMPRESSOR OIL DEGRADATION ASSESSMENT

Radu MIREA[1], Mihaiella CRETU[1], Gabriel TOMESCU[1], Laurentiu CEATRA[1]

ABSTRACT: The aim of the paper is to highlight the influence of natural gas composition on a mineral compressor oil. The compressor oil is HYD HLP68 and it is used in screw compressors for natural gaz compression. Among the all factors that influence the performances of a compressor oil, the composition of the gas to be compressed has the most important influence. Thus, a research related to the degradation of oil during compressor working was made. Base characteristics determinations - flash point and cinematic viscosity were performed as well as FTIR testing for the samples. The degradation tendency of the oil based on FT-IR spectroscopy was assessed. The preliminary conclusions regarding the degradation of base characteristics, emphasizes that the "rich" natural gas has a very important influence on oil's characteristics, thus diminishing its performance.

KEYWORDS: screw compressor, degradation, mineral oil, flash point, FT-IR spectroscopy

NOMENCLATURE

IR – infrared
FTIR – Fourier transform infrared spectroscopy

1. INTRODUCTION

What is specific worldwide for the operation of an oil injected screw compressor is that oil is continuously injected into the compressor, both to cool the gas during compression and to lubricate and cool the compressor's parts, while the most important characteristics required for oil are viscosity, density, flash point, foaming characteristics and acid number [1]. Any lubricant/oil contains the so-called "base oil" (75-85% of the end product) and a set of additives (15-25%) used to enhance the performance of the base oil and to eliminate adverse properties that can be generated during exploitation [2].

There are two main types of base oils: mineral and synthetic. Mineral base oil is derived from the purification of crude oil, whereas the synthetic one is a chemical obtained from contaminant-free pure compounds intended for lubrication tasks. The main component of synthetic base oil is "designed" as a product of a chemical reaction between two or more substances, depending on the desired performance in a specific application, which makes up the major advantage of synthetic lubricants. Their advantages also include resistance to oxidation and high temperature, very good mechanical strength, very good adhesion to lubricated surfaces, all ultimately resulting in significantly higher energy efficiency.

In order to keep a rigorous eye on the operation of the industrial plants, specific sampling strategies are in place (points along critical routes) and regular specific tests are performed [3], [4].

An important part of oil injected screw compressors maintenance programme consists in assessment of oil degradation. Thus, a sample collection programme is issued for each extraction plant. The collected samples are then analysed both from functional: flash point and cinematic viscosity measurement and structural FTIR analysis point of view. The influence of natural gas composition has a great influence in oil degradation. The current paper refers to HYD HLP68 compressor oil, mineral, which is used in Tintea gas extraction location. The site is situated in the southern part of Romania in sub-Carpathian hills. The area is well known for its natural gas deposits. Even though, the deposits are not similar but they have a lot of differences. Thus, the deposit is, so called, a "rich" deposit. The term "rich" refers to the fact that the deposit has other

[1] Romanian Research and Development Institute for Gas Turbines COMOTI, Bucharest, Romania

hydrocarbons along with methane (CH_4).

According to the literature, "rich" deposits have less CH_4 and more C_2-C_7 fractions called gasoline. These gasolines are mainly responsible for the degradation of oils. The matter of developing a specific type of oil for natural gas compression equipment, in Romania, has not been seriously addressed so far, being used only mineral base oils or synthetic PAO base oils having as components that degrade at the same rate. The explanation resides in the natural gas solubility in mineral oils. The gas dissolved in mineral oils leads to a constantly decreasing viscosity and flash point, because it contains molecules similar in structure, mainly C-H bonds, unlike dieter and PAG based synthetic oils, which are polar molecules.

2. PAPER CONTENT

2.1. Determination of base characteristics of the obtained samples

HYD HLP68 compressor oil is a mineral oil which is commonly used for natural gas compression applications with an applicability domain in the areas where the natural gaz deposits are "poor", thus contains less C_2 - C_7 hydrocarbons and more CH_4.

Hydraulic oil HLP69 is a mineral bese oil produced by LiquiMoly and was succesfully used for air and "poor" gas compression. The main purpose of the current paper is to assess the behavoiur of this kind of oil in an oil injected screw compressor which compress a "rich" gas. Thus the oil was put in an oil injected screw compressor deployed at Tintea extraction site and monitored during 3800 working hours.

The paper presents smpling tests made for 900, 2000 and 3800 working hours. The monitored characteristics of the oil were: cinematic viscosity at 40°C, flash point and structural transformations by FT-IR spectroscopy. The obtained values for the viscosity at 40^0C emphasises a 55-64 % decrease and for flash piont a 83-89 % decrease compared with the new, unused sample as seen in table 1.[6,7]

Tabel 1: Obtained values for HYD HLP68 oil

Determined characteristic / Sample	***Viscosity at 40 °C, [mm²/s]***	***Flash point, [C]***
Method	*SR ISO 3104-2002*	*ASTM D92 - 05a*
Equipment	*SCAVINI equipment Ubbelohde COMECTA*	*SCAVINI equipment*
Values according to technical sheet BASF TI/EVO 0010 e / Nov. 2015	**68**	**240**
900 h	30.7	40.7
2000 h	24	27.3
3800 h	23.4	26.8

2.2. FTIR tests of the obtained samples

Fourier transform infrared (FTIR) spectroscopy is a versatile tool used to detect common contaminants, lube degradation by-products and additives within lubricating oils. It has become a widely used technique for quickly assessing multiple lubricant characteristics. This test method is relatively quick to perform and is capable of simultaneously detecting multiple parameters, including antioxidants, water, soot, fuel, glycol, oil oxidation and certain additives. Adding to the power of this qualitative measurement, the size of the peaks is a direct indication of the amount of the specific material found in the sample. Since most used oil samples are complex mixtures of thousands of different molecules, including base oil molecules, additives, oil degradation by-products, wear debris and contaminants, the infrared spectrum of the sample is typically complex and can be difficult to interpret with any degree of certainty, as some wave numbers may overlap. Despite these drawbacks, FTIR still has great value in used oil analysis and is employed by the majority of oil analysis labs as a screening tool. [5]

The tests have been performed within Physical-Chemical Determination lab on a FTIR Spectrum Oil Express Series 100, v 3.0 spectrometer provided by Perkin Elmer which has an auto sampler. (fig. 2)
The equipment is specially designed for FTIR analysis of used oils, made of: sample purge compartment, optical system in spectral domain 7800-370 cm^{-1} having a resolution of 0.5 cm^{-1}, intermediary IR detector, electronic system with signal processor Motorola DSP56303 and Motorola 68340, PC, Spectrum Software, auto sampler. The used solvent is n-heptane. The spectrometer is capable of displaying the results both in for of absorbance or transmittance. Absorbance (A/cm) is the most used way of displaying the results since is proportional with the concentration of the specific funcyional group within the sample [8]. As is shown in table 2, after analysing the results, it can be observed that there are some differences between tested samples. After analysing the quantitative results, it can be observed the water content slightly increases as well as OH groups. There are traces of oxidation of the nitrogen groups (NO_x) which are mainly found in the anti-wear additive. SO^4 groups are also present in the oil and are correlated with sulphatation of the oil.

Fig. 2 Spectrum Oil Express Series 100, v 3.0

Table 2. FTIR results for HLP HYD68

Characteristic	**HLP HYD68 K1 - 900 h**	**HLP HYD68 K1 - 2000 h**	**HLP HYD68 K1 - 3800 h**
Anti-wear (A/cm)	0.61	0.55	0.26
Hydroxi (A/cm)	0	0	0.68
NOx (A/cm)	2.35	2.2	1.58
NOx vs Oxid (A/cm)	4.45	7.77	2.32
Oxidation (A/cm)	1.18	3.21	1.26
Soot 1980 (A/cm)	0.06	0.36	0
Soot 3800 (A/cm)	2.29	2.19	1.14
Sulf vs. Oxid (A/cm)	6.72	10.48	3.38
Water (%)	0	0	0.02

3. CONCLUSIONS

- As a result of sample analysis as shown in tables 1 and 2, it can be seen that the values of base characteristics (cinematic viscosity and flash point) are far from the ones stated in the technical datasheet of the oil.
- Table 2 shows the changes within the chemical composition of the oil during its working period: anti-wear additives are almost finished, nitrous and sulphating occurs and also soot particles.
- After analysing FT-IR spectra, it is clearly highlighted that at 3800 working hours, there are more short carbon chains in the structure of the oil due to the fact that the gasoline which are present in the "rich" gas are continuously affecting the long carbon chains of the oil. Also, the presence of gasoline (C_3 - C_7) in the compressed gas makes them accumulate in the oil.

4. ACKNOWLEDGEMENTS

The research has been carried out within Program Nucleu, project PN 19.05.02.02, financed by Romanian Ministry of Research and Innovation.

5. References

[1] ***_Physical Properties of Lubricants_, Engineering Tribology, Tribology Series Vol. 24, 1993, Pp 11–57
[2] *** _Componenta lubrifiantilor_, http://www.xoil.ro/lubrifianti/tribologie/
[3] Vidrighin C., "_Strategii pentru evaluarea analitică a lubrifianţilor industriali_", 2013, http://www.ttonline.ro/autori/costin-vidrighin
[4] Vidrighin C., "_Programe de analiza a lubrifiantilor_", 2013, http://www.ttonline.ro/autori/costin-vidrighin]
[5] Wright J. _"Benefits of FTIR oil analysis"_, Machinery lubrication, no. 8/2015
[6] *SR EN ISO 3104:2002/AC:2002 - Produse petroliere. Lichide opace si transparente. Determinarea viscozitatii cinematice si calculul viscozitatii dinamice;*
[7] *SR EN ISO 2592:2018 - Petrol şi produse conexe. Determinarea punctelor de inflamabilitate şi de aprindere. Metoda Cleveland cu vas deschis;*
[8] *Determinarea gradului de uzură a lubrifianţilor, prin analiza FTIR*

LOX/LCH4 UPPER STAGE DEVELOPMENT STRATEGIES FOR FUTURE LAUNCHERS

Theodora ANDREESCU[1], Andreea MANGRA[1], Valeriu VILAG[1], Ion MALAEL[1], Alexandru CANCESC[1], Jeni VILAG[1], Dan IFRIM[1], Simona DANESCU[1]

ABSTRACT: The reduction of Earth-to-orbit launch costs in conjunction with an increase in Launcher reliability and operational efficiency are the key requirements of future space transportation systems. This paper underlines the progress in LOX/CH4 upper stage engine development carried out by COMOTI and also being provided the prediction of the rocket engine performances at the conceptual and preliminary stages of design. This paper focuses on the trade-off studies for the engine architecture definition, considering both open and closed thermodynamic cycles. Various subsystems configurations have been taken into account, analyzing the optimum configuration in terms of performance. The main operating and geometrical parameters were discussed: combustion pressure, optimum mixture ratio, turbine pressure ratio, thrust chamber geometry, and the turbopump size is addressed.

KEYWORDS: upper stage, liquid rocket engine, turbopump, LOX/CH4 cryogenic propellant, thrust chamber

NOMENCLATURE

A – turbine characteristic area
A_e - nozzle exit diameter
A_t – nozzle throat diameter
A_c – combustion chamber area
T_c – combustion temperature
γ - specific heat ratio
C_p- specific heat capacity
p_c – combustion pressure
C_F – thrust coefficient
c^* - characteristic velocity
g_0 – gravitational constant
x_{pf}, x_{pm}, - axial width
$\dot{m}$ – gas flow rate
P_{pox} – liquid oxygen pump power
P_{pfuel} – liquid methane pump power
P_T – turbine power
n_s – pump specific rotational speed
α – turbine flow angle
σ_p^* - turbine pressure losses
R – gas constant
ρ – density
M – Mach number
h_{pf}, h_{pm} – turbine blades hight

1. INTRODUCTION

As the present trend in rocket engine development recommends a high versatility and low launch service cost, while preserving high performance, expander cycle upper stage based on LOX/LCH4 being a key competitiveness factor recognized by the market. The new ESA-VEGA Development Program aimed at improving the VEGA competitiveness throughout three major high-level objectives: decrease of the Vega C Yearly Launch System Service Cost for lower price per launch into the reference orbit with a target of 10% as cost reduction in production and operations, Increase of the VEGA C Launch System Margins for higher mission flexibility complementarily with Ariane 6 Launch System and to Increase of the VEGA C Launch System Services Versatility for ad-hoc launch services solutions based on available products, including small spacecraft mission services (SSMS-C), dual – launch services (VESPA-C) and orbit transfer services (VENUS). Also, the introduction of VEGA-C that cover large part of the LEO payloads has led to focus main motivations for VEGA-EVO of the following main drivers:

[1] Romanian Research and Development Institute for Gas Turbines COMOTI, Bucharest, Romania

- Competitive: recurring Cost 20% less than VEGA C target price;
- Green: elimination of all the toxic propellants;
- Flexible: multiple altitudes and orbital planes;
- Scalable: a family of launchers suitable for different payloads.

As regards the upper stage, there is a pronounced need to develop a new class engine based on "green propellant" and relatively low power due to the development of low-costs and environmental options. The main distinguishing properties of the upper-stage compared to the first stage engines are as follows: the engine must start in a vacuum, while engines of previous stages continue to operate; the specific impulse must increase by using high-nozzle area ratios.

Fully cryogenic LOX/LCH4 is one of the most promising liquid-rocket-engine technologies due to the following advantages: reduced dry mass, compact architecture, cooling capabilities, reusability issues and mission flexibility. [4]

Methane is a soft cryogenic that is not corrosive and has low toxicity, therefore being easier to store, requires less insulation and fewer concerns than hydrogen fuel systems. Also, liquid methane is about six times denser than hydrogen; thus methane tanks require a smaller storage volume than comparable hydrogen tanks. Furthermore, methane has exceptional heat capacity properties that provide good cooling properties for expander cycle; methane fuel has lower pressure drops in regenerative cooling channels compared to kerosene fuel. In addition, methane is natural gas, being 5 to 10 times cheaper to acquire and store than liquid hydrogen. [18]

The highest risk involved in the expander cycle engine development is to match the coolant circuit capability to the engine requirements. The working pressure inside the combustion chamber imposed a sufficient amount of heat to be extracted from the coolant circuit to power the turbomachinery while still providing a suitable cooling in order to avoid structural damages. This risk can be mitigated through numerical analysis, combustion chamber components testing and engine test bench experimental testing. Any variation in the extracted energy can be controlled through orifices to adjust the distribution of flow between the combustion chamber and the turbine.

None launcher upper stage based on the combination LOX/LCH4 has yet flown, but ground testing of such systems is being carried out, as an example, the upper stage LM10-MIRA foreseen for the evolution of VEGA-E launcher.

Aim of the current study is to evaluate the performance of an oxygen/methane expander system intended to the upper stage with a specific focus on thrust chamber and feeding system design.

The clean-burning, non-toxic, high vapor pressure propellants provide significant advantages for reliable ignition in space. The main components in a cryogenic upper stage engine are the thrust chamber assembly; the propellant feed control system, the turbopumps, the propellant tank pressurization system, the electrical system, the hydraulic control system and the flight instrumentation system.

A liquid rocket upper stage can be divided into two main parts: a feeding system and thrust chamber assembly. The feeding system suitable for this type of application is based on turbopumps that are designed to provide the required energy to the propellant for an optimum combustion process. Another technique to characterize the engine cycle is based on the turbine and thrust chamber arrangement, the cycle is classified as open or closed. Advantages of a well-established power cycles include lower development cost, reduced development risk, repeatable starts and a compact assembly.

For each configuration, the following design steps were performed:

- Definition of the engine operational parameters;
- Thrust chamber geometry definition;
- Pump concept design;
- Turbine concept design.

This procedure allows estimating the engine performance based on sub-systems concept design procedure. For higher performance, mechanical pumps must be used to feed the combustion chamber.

2. LIQUID ROCKET ENGINE CYCLE DESIGN

Considering a thrust range of $30kN$, a LOx / CH4 cycle analysis was performed to determine the most performant global architecture. The investigation has been channeled on three directions: gas generator cycle, staged combustion cycle (both fuel-rich and oxidizer-rich) and expander cycle. This analysis allows selecting thrust chamber performance, turbopump assembly power, thrust chamber size and cooling system configuration.

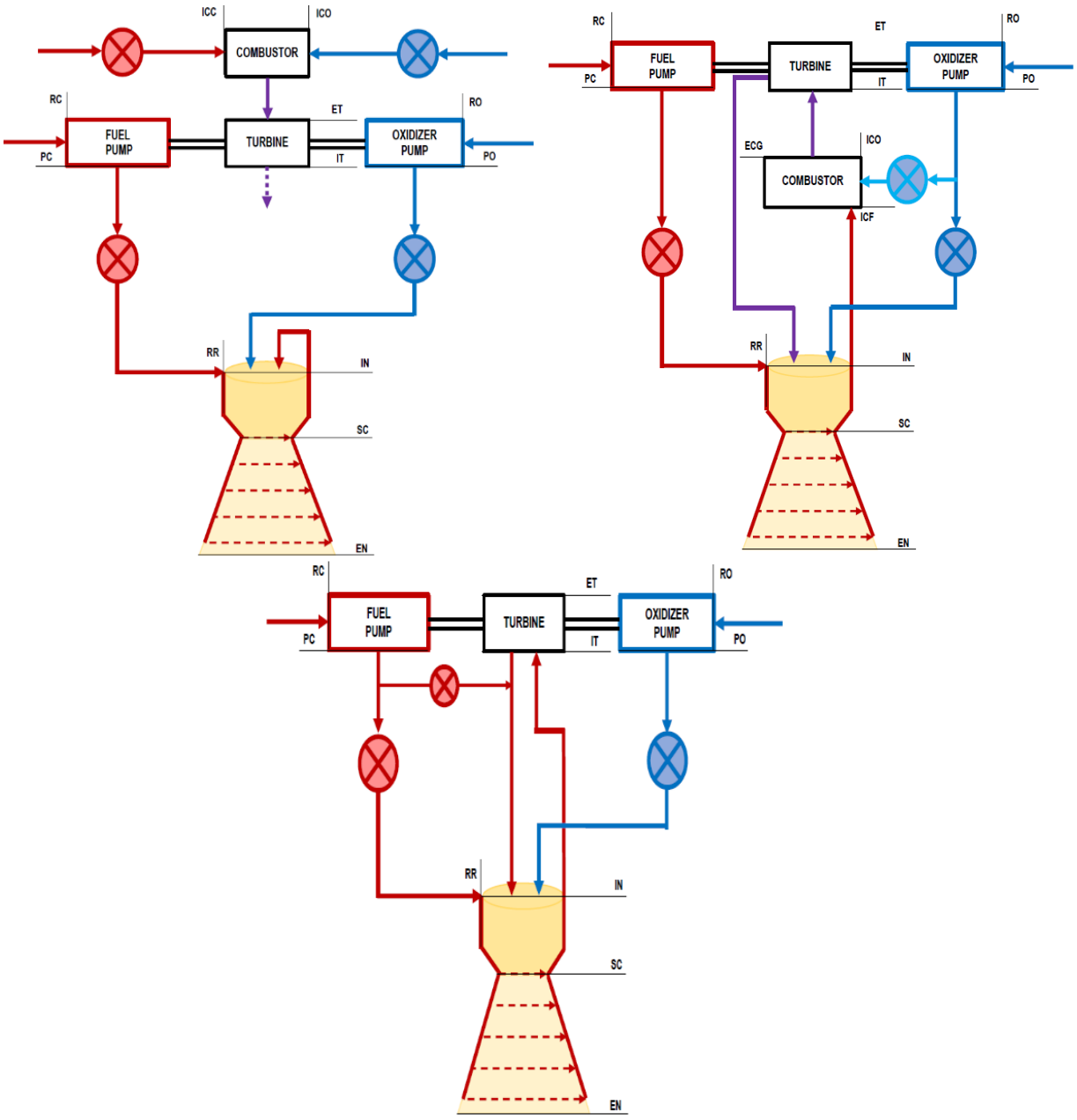

Fig.2.1 a) Rocket Engine Cycle with Gas Generator, b) Staged-Combustion, c) Expander Cycle,

In the Gas Generator Cycle (Fig2.1.a) a small fraction of the pressurized oxidizer and fuel are directed through a medium-temperature burner (Gas Generator) which therefore produces a fuel-rich gas to drive the turbine. These are designed with large pressure ratio and the remnant gases are usually reintroduced in the exhaust nozzle, after the critical section in order to assure extra thrust.

For engines, utilizing hydrogen or methane as fuel, the gas generator could be replaced. Therefore, the fuel could be routed from the exit manifold of the nozzle cooling circuit to the turbine inlet. This could be possible because methane behavior is supercritical at the pump exit and follow a simple expansion procedure as gains heat. The resulting expander cycle is compact and efficient because all amount of fuel is used in the thrust chamber. The principal limitation of the cycle is the relatively small amount of heat available from the regenerative cooling, which limits applicability to combustion pressures under 7MPa. [5]

For rockets with high chamber pressure, the staged combustion cycle is the optimum solution. A small amount of oxidizer is added to the fuel after the cooling circuit

For any cycle, the pump must meet the pressure and flow rate requirements of the turbine while in turn it should drive the pump within the pressure ratio limitation. Through upper stages with Gas Generator Cycle the combustion chamber pressure generally are maintained below 10MPa in order to avoid high turbine flowrates.

A pump-fed rocket engine with turbine extracted from the cooling system is referred to an expander cycle, being intended for upper-stage, considering its limitation in terms of available power when compared to staged-combustion and gas generator cycles. The absence of gas generator allows for easier start-up sequences and avoids the controlling of the mixture ratio of the gas generator. From other points of view, the expander cycle is not suitable for high thrust level, due to the limitation imposed by the power that could be extracted from the cooling process of the thrust chamber.

In the Expander Cycle (Fig. 2.1.c) the chamber pressure is limited due to the amount of heating available for the turbine working fluid. [5] At the same imposed combustion pressure, the expander cycle requires a higher pump discharge pressure. For the stage-combustion cycle, the chamber pressure could attain a chamber pressure of about 20MPa because the preburner provide high-energy working fluid for the turbine [16]; 20MPa is actually an upper limit for the turbine drive cycle because for a given turbine inlet temperature and turbopump efficiency, the required pump discharge pressure rises at higher quotations. Expander cycles are reliable and have multiple restart capability, while the LOX/LCH4 offers high specific impulse with attractive bulk density and handling characteristics [19].

For the Gas Generator Cycle, turbine pressure ratios of about 20 are required in order to minimize the flow rate of the turbine working and therefore maximizing the specific impulse. For the expander and staged-combustion cycles, the optimum turbine pressure ratios are typically less than 1.5, because of the large turbine working fluid available. For that configuration, turbopump assembly weight is greater comparative to expander and staged-combustion cycle. These differences originate from pump discharge pressure differences. In order to gain high system efficiency, pumps in expander and staged-combustion cycle either operate at higher speed or have more stages than those in the gas generator

2.1 CASE STUDY

Recent studies for new generation upper stage cryogenic engines in Europe with the main goal to increase the reliability and performance, have engines with restart capability and low development costs identify expander cycles as a promising technology. The main elements of an expander cycle are a tank system, turbopump system, cooling system, injector system, main combustion chamber and exhaust nozzle [1].

For this type of technology, the heat exchange by regenerative cooling is a critical point in expander cycles as the hot gases formed need to drive the turbine. When is used a regenerative cooling technique, the coolant, which is the fuel because oxidizers at high temperature lead to corrosion issues, is passes in cooling channels along with the thrust chamber before it is redistributed into the combustion chamber [17]. The major limitation is the relatively low achievable combustion chamber pressure level, which ultimately limits the maximum thrust level. Therefore, the expander cycle is a proper candidate for an upper stage.

The LOX/LCH4 engine mixture ratio has been set to 3.36 in order to minimize the turning inlet temperature to 1100 K and to be far from the stoichiometric ratio. In order to avoid the two-phase flow in the cooling circuit, for the LCH4 case, the pressure must be higher than the critical pressure, of 45.9 bars. [16]

For this study, considering the potential of a higher density of liquid methane compared to liquid oxygen, a system with a single turbine acting both fuel and oxidizer pumps is considered. For an optimized cooling of the thrust chamber, the total mass flow rate flows in the cooling system.

3. PERFORMANCE EVALUATION AND THRUST CHAMBER PRELIMINARY DESIGN

Fuel, oxidizer and mixture ratio determines the start characteristics of the flow field in the combustion chamber and further the chamber geometry influences the nozzle performance. In this paper, it has been analyzed how a combustion pressure in 1-10MPa influences the mixture ratio choice for LOX/CH4 combination. Also, an expansion ratio (A_e/A_t) with a variation in the range of 10 – has been investigated.

The specific heat ratio(γ), the combustion temperature (T_c), the molar mass, the density and the specific heat capacity (C_p) for mixtures of fuel and oxidizer were obtained from CEA. From the specific heat ratio, the value of the Van Kerckhove function Γ [2] was calculated:

$$\Gamma = \sqrt{\gamma}\left(\frac{2}{\gamma+1}\right)^{\left(\frac{\gamma+1}{2(\gamma-1)}\right)} \tag{3.1}$$

The Mach number (M) at any point in the thrust chamber could be found from solving the area-Mach number relation:

$$\left(\frac{A}{A_t}\right)^2 = \frac{1}{M^2}\left[\frac{2}{\gamma+1}\left(1+\frac{\gamma-1}{2}M^2\right)\right]^{\frac{\gamma+1}{\gamma-1}} \tag{3.2}$$

The performance parameters such as thrust coefficient C_F and characteristic velocity c^* could be expressed with the following relationships [1]:

$$C_F = \Gamma\sqrt{\left(\frac{2\gamma}{\gamma-1}\right)\left(1-\left(\frac{p_e}{p_c}\right)^{\frac{\gamma-1}{\gamma}}\right)}+\left(\frac{p_e}{p_c}-\frac{p_a}{p_c}\right)\frac{A_e}{A_t} \tag{3.3}$$

$$\mathrm{c}^* = \frac{\sqrt{\gamma \mathrm{R} T_c}}{\Gamma} \tag{3.4}$$

Knowing the thrust coefficient and characteristic velocity allows calculating the thrust chamber specific impulse:

$$\left(I_{sp}\right)_{ideal} = \frac{F}{g_0 \dot{m}} = \frac{C_F \mathrm{c}^*}{g_0} \tag{3.5}$$

Selecting the design point chamber pressure is a key decision in the development of a new rocket engine. Higher chamber pressure generally enables higher impulse. For an expander cycle, selection of the chamber pressure is important since the extracted power to operate the turbopump system is extracted from the combustion chamber cooling circuit.

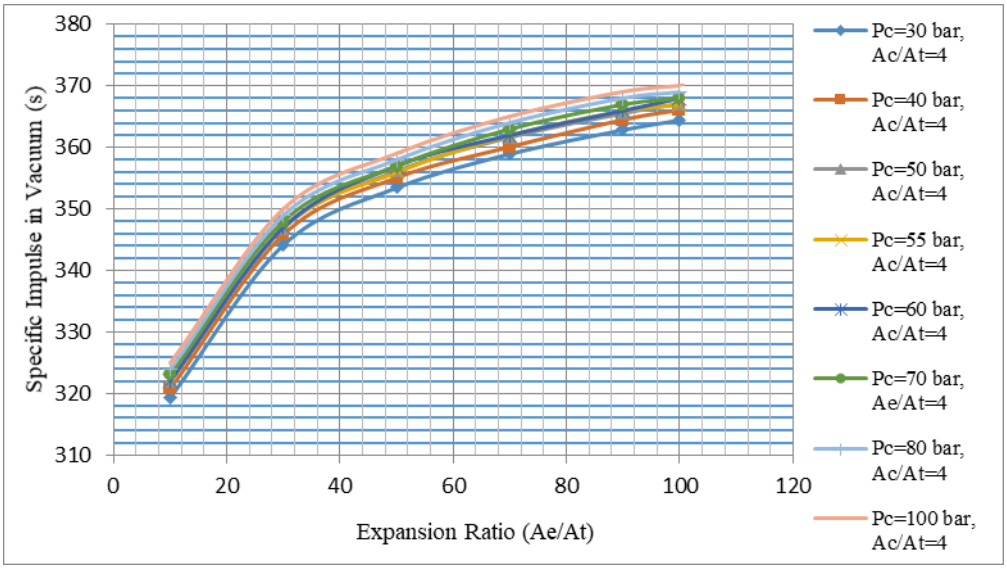

Fig. 3.1 Specific impulse function of expansion area ratio for different combustion pressures

For Fig. 3.1 representation of the LOX/LCH4 engine mixture ratio has been set to 3.36 and the exit pressure to 0.01 bar. Nozzle exit conditions such as exit pressure, temperature or density are unknown; therefore, the change in conditions in the nozzle was performed step by step starting from the throat towards the nozzle exit. Therefore, the nozzle calculations have been done by dividing the nozzle into segments.

Through the performance evaluation section, for a thrust range of 30 kN imposed and LOX/LCH4 as propellant, the combustion pressure was varied in the range of 3-10MPa, with a step of 10, the compression area A_c/A_t between$1.2 \div 6$, with a step of 1 and expansion ratio A_e/A_t between$10 \div 100$, with a step of 10.

By varying all these operating parameters, it is intended to obtain a thrust chamber mass as small as possible, taking into consideration a specific impulse I_{sp} within the 370 s range.

After numerical investigation, it could be shown (fig.3.1) that the specific impulse increases with the expansion area ratio A_e/A_t. After ratios greater than $A_e/A_t > 70$ the specific impulse grown rate is not pronounced. Also was demonstrated that the area contraction ratio does not influence the specific impulse which slightly increases with combustion pressure.

For what concern the thrust chamber dry mass is related by the following relation:

$$m_{engine} = (0.001F + 49.441)N^{0.03}(A_e/A_t)^{0.004} \text{ [16]} \tag{3.6}$$

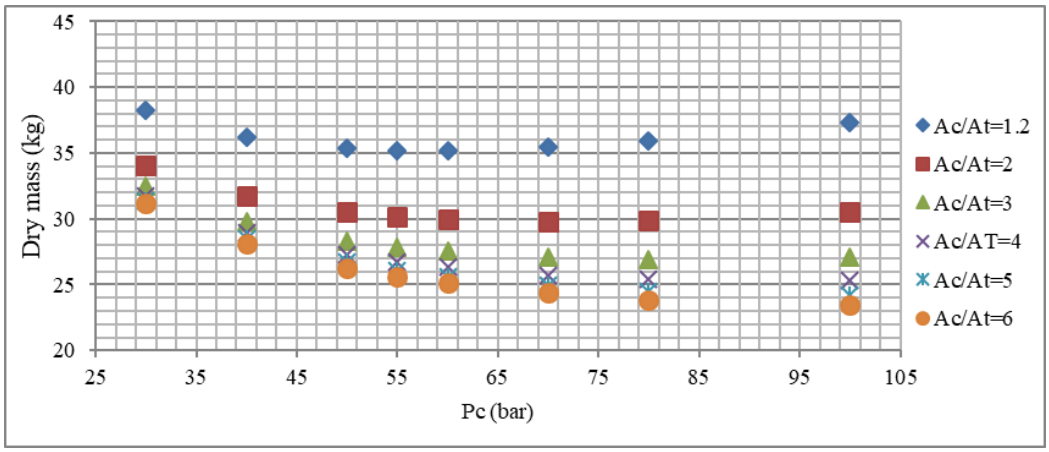

Ae/At=30

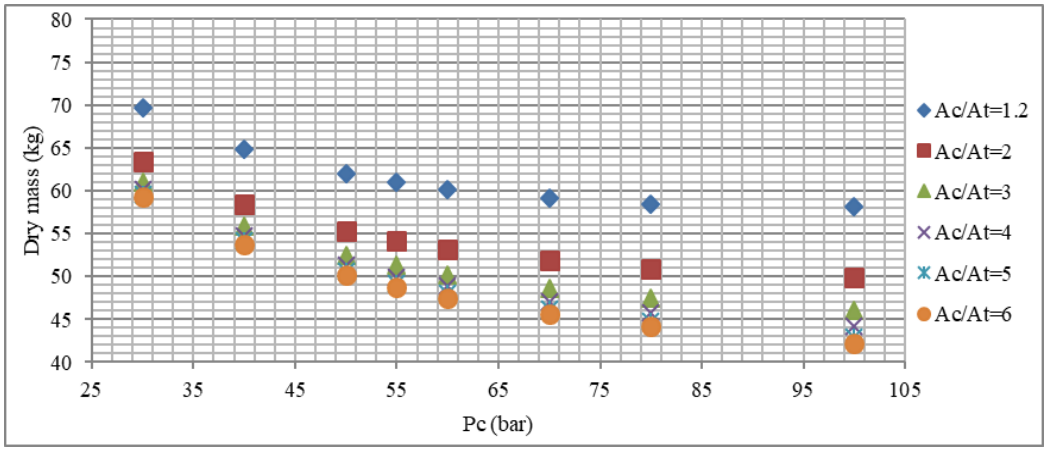

Ae/At=60

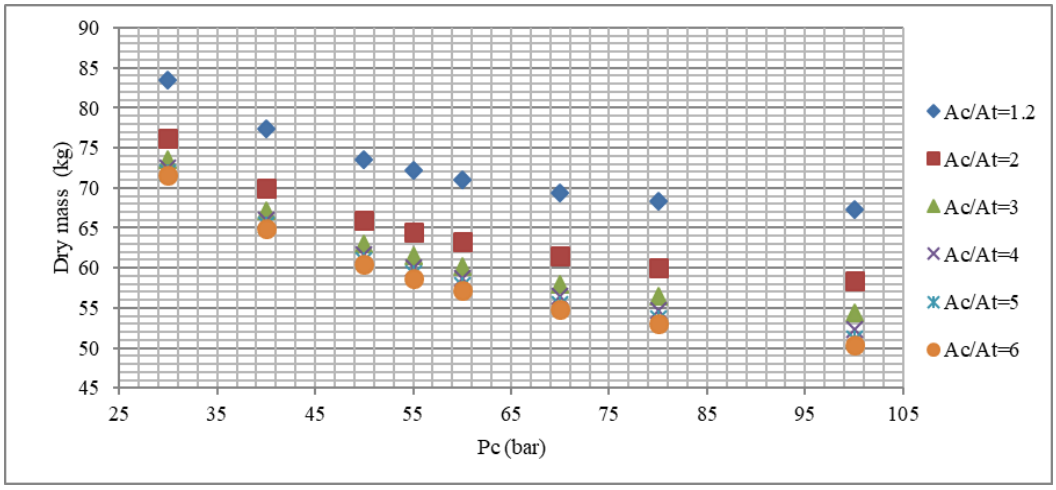

Ae/At=90

Fig. 3.2 Thrust Chamber mass dependence on P_c, A_c/A_t, A_e/A_t

Fig. 3.2 presents the variations on the dry mass of the thrust chamber. It can be seen that the mass of the combustion chamber and nozzle decrease as chamber pressure increases. This is expected because as chamber pressure increases, the throat shrinks for a given desired thrust and expansion ratio. Regarding turbopump, assembly mass is proportional to the power required by the turbine. As the combustion chamber pressure increases the power needed from the turbine increase to provide the pressure rise and consequently the overall turbopump assembly mass increases.

A high specific impulse is desired in trying to achieve a high-performance upper stage. Since expansion ratio increases the engine diameter increases, this was the limiting factor in choosing the expansion ratio. Given the specific limitations on exit diameter for upper stage engines, an expansion ratio of 60 was chosen.

From the graphics exemplified besides, thrust chamber mass increase significant with expansion area ratio and decrease with A_c/A_t increment; the decrease is not as significant for the values $A_c/A_t > 3$.

Also, the thrust chamber mass decreases as the pressure increases in the combustion chamber. The minimum take-off mass was taken as an objective function. Since launcher development costs tend to vary as a function of gross take-off mass; therefore, minimum gross take-off mass vehicle may be considered as a minimum development cost concept.

The optimization function related to LOx/LCH4 upper stage performances is given by:

$$C = 0{,}5 \cdot \frac{m_{ref}}{m} + 0{,}3 \cdot \frac{V_e}{V_{e\,ref}} + 0{,}2 \cdot \frac{I_{sp}}{I_{sp\,ref}} \tag{3.7}$$

where m_{ref} = 30.9502 kg, V_{eref} = 3532.721 m/s, I_{spref} = 360.2373 s.

The current analysis has been performed for a fixed engine thrust of $30kN$, combustion chamber pressure variable in the range 60-100 bar, expansion ratio between 10-100 and contraction ratio in the range 1.2-6. Our starting point for this analysis is the determination of the mass of the engine, being at the same time correlated with thrust. We determined, therefore, an optimum mass for a given thrust function on different operational parameters.

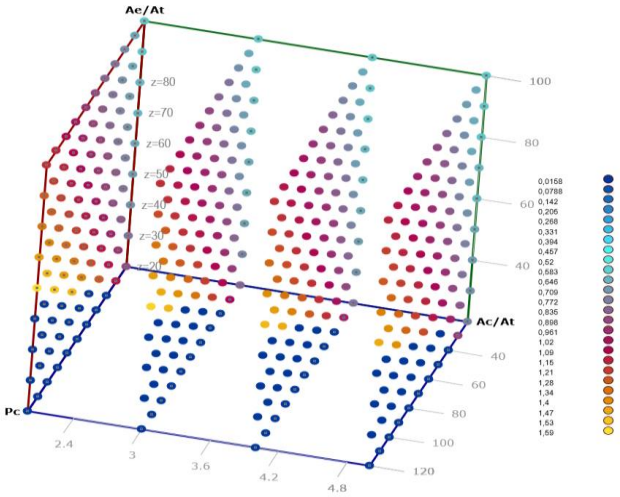

Fig. 3.3 Parametric investigation of LOX/LCH4 upper stage performance and the distribution of imposed criterion

With the objective of obtaining a smaller mass but at the same time a specific impulse as close to 370 s, it was chosen as the optimal combination: $P_c = 60\ bar$, $A_c/A_t = 4$ and $A_e/A_t = 60$.

For the full cryogenic upper stage design mainly focuses on determining the basic dimensions of the engine (Table 3.1). For this type of application, a cylindrical combustion chamber with converging-diverging exhaust nozzle.

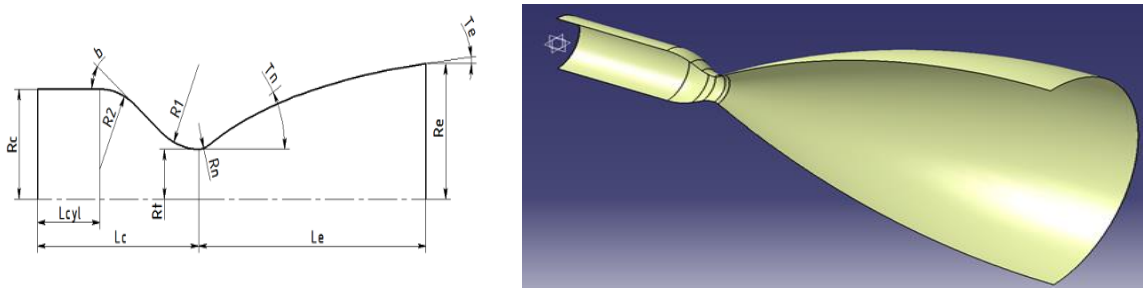

Fig. 3.4 Preliminary design of the thrust chamber

Table 3.1 Thrust chamber preliminary design parameters

Thrust (ken)	30	**Lcyl (mm)**	197.19
Combustion pressure (bar)	60	**R1 (mm)**	43.16
Mass (kg)	43.65	**R2 (mm)**	85.5
Specific Impulse (s)	360	**b (deg)**	30
Total flow rate (kg/s)	8.5368	**Dt (mm)**	57.55
Oxidizer flow rate (kg/s)	6.58137	**Rn (mm)**	10.99
Fuel flow rate (kg/s)	1.95542	**Tn (deg)**	35.75
Dc (mm)	115.09	**Le (mm)**	606.48
Lc (mm)	281.59	**Te (deg)**	8

Maximizing the specific impulse in an upper stage has a greater positive effect on payload capacity. Chamber and nozzle heat transfer scales proportionally with surface area exposed to combustion products. The surface area of a nozzle is proportional to the chamber diameter. For a constant chamber length, the heat transfer increases with the square root of the throat area. In order to minimize this effect, the chamber length could be gradually increased, but this will reduce the allowed nozzle length and area ratio (for a fixed engine length), increase the chamber coolant pressure losses and increase engine weight. Therefore, considering that the total heat transfer does not scale proportionally with increased thrust, expander cycle chamber pressure decrease as the thrust range is increased.

4. LOX/LCH4 TURBOPUMP SYSTEM

In the expander cycle, the power required to drive the pumps is proportional to propellant flow rates and pressure rise. In order to have low pressures in the storage tanks but still have high pressures in the combustion chamber a pump system is needed to increase the propellant pressure. Therefore, the component modeling goal is to increase the oxidant/propellant pressure and determine the power needed to achieve this.

This effort details the design of LOX and CH4 pumps required by an expander cycle upper stage engine. Materials must be found than can tolerate LOX and LCH4 (inducer and impeller). The impeller and diffuser must be designed in such a way to maximize throttle ability. [5]

The pump component determines the required pump power. It could be deduced from the mass flow passing the pump, the required pressure rises over the pump, the density of the propellant and efficiency of the pump. The LOX/LCH4 pumps follow from [16]:

$$P_{pox} = \frac{1}{\eta_{pox}} \dot{m}_{ox} \frac{\Delta p_{ox}}{\rho_{ox}} \tag{4.1}$$

$$P_{pfuel} = \frac{1}{\eta_{pfuel}} \dot{m}_{fuel} \frac{\Delta p_{fuel}}{\rho_{fuel}} \tag{4.2}$$

More specifically the power balance can be written as:

$$\frac{1}{\eta_{pox}} \dot{m}_{ox} \frac{\Delta p_{ox}}{\rho_{ox}} + \frac{1}{\eta_{pfuel}} \dot{m}_{fuel} \frac{\Delta p_{fuel}}{\rho_{fuel}} = \eta_T \dot{m}_T C_p T_{in} \left(1 - (p_{out}/p_{in})^{\frac{\gamma-1}{\gamma}}\right) \tag{4.3}$$

The pumps designs involve a large number of interdependent variables. This section outlines some of the key parameters and features that have been considered in the design of LOX/LCH4 pumps.

The required pumps flows are established by the rocket design, exhaust gas velocity, propellant densities and mixture ratio. Also, the pumps discharge pressures are determined from the chamber pressure and hydraulic losses in valves, lines, cooling jacket and injectors.

As a first step it was determined the specific rotational speed with the following relation [10]:

$$n_s = 3.65n \frac{\sqrt{Q}}{H^{3/4}} \tag{4.4}$$

The inlet and outlet rotor diameter could be determined by the aid of the following relations:

$$D_1 = (1.1\sim1.5)K_0\sqrt[3]{\frac{Q}{n}} \tag{4.5}$$

$$D_2 = 19.2\left(\frac{n_{sopt}}{100}\right)^{1/6}\sqrt{\frac{2gH}{n}} \tag{4.6}$$

The exit rotor blade high is given by:

$$b_2 = 0.78\left(\frac{n_{sopt}}{100}\right)^{1/2}\sqrt[3]{\frac{Q}{n}} \tag{4.7}$$

Blade number:

$$Z = 6.5\frac{D_2 + D_1}{D_2 - D_1}sin(\beta_1 + \beta_2) \tag{4.8}$$

Also another important parameter is the net pressure suction head [13]:

$$NPSH = \frac{p_{inlet} - p_{vapour}}{g_0\rho} \tag{4.9}$$

Using ANSYS Vista CPD the two pumps were pre dimensioned. Among the required data are speed, gas flow rate, working fluid density, pumping head, inlet flow angle and velocities ratio.

Table 4.1 Pumps inputs design parameters

LOX Pump		**LCH4 Pump**	
Rotational speed (rpm)	30850	**Rotational speed (rpm)**	30850
Volume flow rate (m^3/h)	20.783	**Volume flow rate (m^3/h)**	16963
Density (kg/m^3)	1140	**Density (kg/m^3)**	415
Head rise (m)	689	**Head rise (m)**	1880
Inlet flow angle (deg)	90	**Inlet flow angle (deg)**	90
Merid velocity ratio	1.1	**Merid velocity ratio**	1.1

Table 4.2 LOX/LCH4 rotor`s main parameters

LOX Pump		**LCH4 Pump**	
Power (kW)	121.8	**Power (kW)**	161.4
Head coeffi	0.430	**Head coeffi**	0.490
NPSH (m)	36.73	**NPSH (m)**	31.78
Impeller inlet D1 (mm)	22.1	**Impeller inlet D1 (mm)**	23.0
Impeller exit D2 (mm)	77.2	**Impeller exit D2 (mm)**	120.1
B2 (mm)	4.7	**B2 (mm)**	6.1

For full cryogenic $30\,kN$ upper stage we have selected a closed expander engine cycle. For that architecture, the turbine that controls the pump is driven by hot gaseous fuel after it has passed as a liquid the nozzle where it is used for cooling. After the gaseous fuel has passed the turbine it is injected into the thrust chamber.

Rocket turbine pumps typically use impulse turbines with higher pressure ratios and higher speeds in order to achieve a compact geometry but affecting the TPO assembly efficiency. For an expander cycle it is preferable to use one stage turbine. [7]

The turbine must provide required shaft power for driving the LOX/LCH4 pumps at a predefined rotational speed and torque. In an impulse turbine, the enthalpy of the working fluid is converted into kinetic energy within the first set of stationary turbine nozzles. The power supplied by the turbine is given by: [8]

$$P_T = \eta_T\dot{m}_T\Delta h = \eta_T\dot{m}_T C_p T_{in}\left(1 - (p_{out}/p_{in})^{\frac{\gamma-1}{\gamma}}\right) \tag{4.10}$$

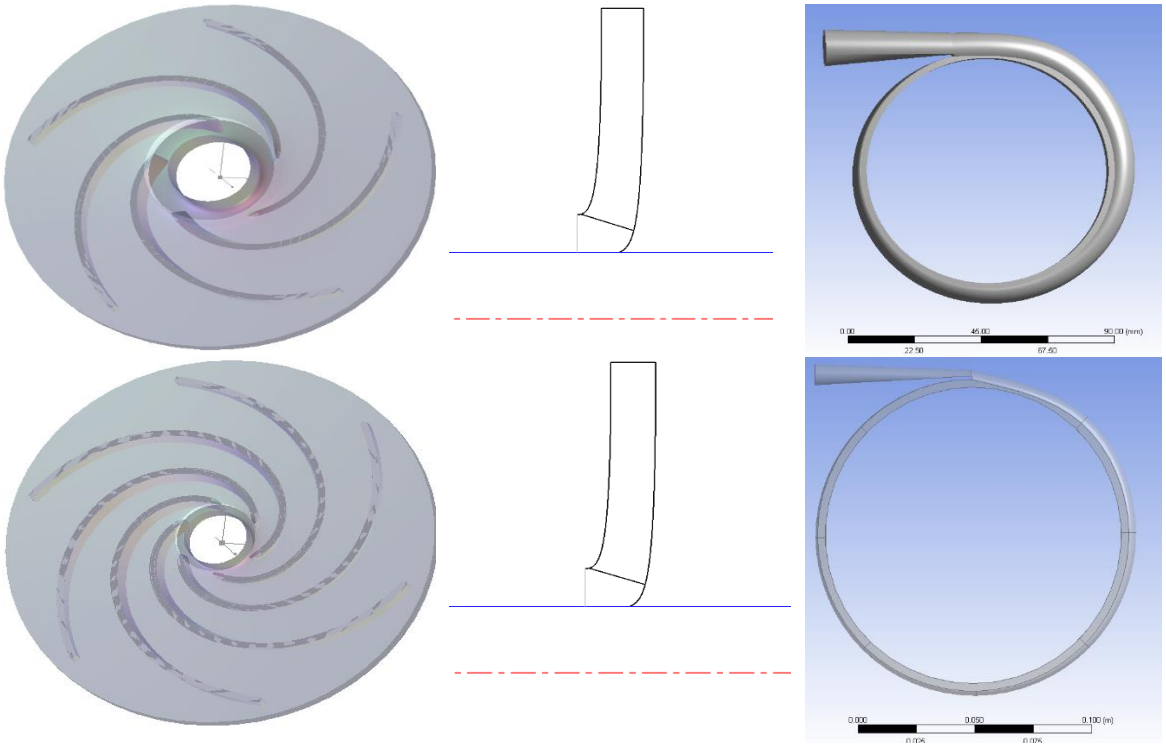

Fig. 4.1 a) LOX rotor pump and volute, b) LCH4 rotor pump and volute

The power delivered is proportional to the turbine efficiency η_T, the fuel flow rate through the turbine nozzles $\dot{m}_T$ and the available enthalpy dropΔh. On the other hand, the enthalpy is a function of the propellant specific heat, the pressure ratio across the turbine and the ratio if the specific heats of the turbine gases. From the power point of view, turbine should cover the power required by the LOX/LCH4 pumps, by the auxiliaries and power losses in the bearings and seals. Innovative blade materials (monocrystals with unidirectional solidifications) or special alloys can assure high inlet temperature in the range 1400-1600K with the additional effects of a higher enthalpy that reduce the required turbine flow. From the cost reduction point of view the actual inlet temperature is limited in the range of 900-1100K [7]. Up to now, the turbine efficiency has a limited value around 0.723 [16], being dictated by centrifugal pump design considerations which limit the shaft speed for turbopumps assembly. For a good design practice, the turbine inlet temperature should be part of the optimization process. For an expander cycle the temperature upper limit is set to 1350 K, but in order to avoid overheating, the suggested design turbine inlet temperature is 1000 K.

For turbine design it will be imposed as input parameters the following: inlet pressure and temperature, gas flow rate, rotational speed and at least outlet pressure and temperature. On the other hand has been defined the turbine power, efficiency and geometrical constraints. The working channel dimensioning is achieved by calculating the areas in the turbine sections. The turbine input energy state is defined by the calculation of the specific enthalpy according to temperature and pressure as well as the working fluid. From continuity equation [9]:

$$\dot{m} = A \cdot sin\alpha \cdot \sigma_p^* \cdot \frac{P^*}{\sqrt{R \cdot T^*}} \cdot \sqrt{\frac{k \cdot M^2}{\left(1 + \frac{k-1}{2} \cdot M^2\right)^{\frac{k+1}{k-1}}}}, \tag{4.11}$$

results the characteristic area:

$$A = \frac{\dot{m}}{sin\alpha \cdot \sigma_p^* \cdot \frac{P_2^*}{\sqrt{R \cdot T_2^*}} \cdot \sqrt{\frac{k \cdot M^2}{\left(1 + \frac{k-1}{2} \cdot M^2\right)^{\frac{k+1}{k-1}}}}} \tag{4.12}$$

To determine the work channel dimensions, the radius at the base of the blade is required and the radius at the top is deduced from the previously calculated area. It is also possible to impose the radius at the top and determine in the same way the radius at the base. At this stage of design the axial is determined by the following empirical relations:

$$\frac{h_{pf}}{x_{pf}} \in (1.3 - 1.5), \tag{4.13}$$

and

$$\frac{h_{pm}}{x_{pm}} \in (2 - 5) \tag{4.14}$$

It was checked that the divergence angle of the channel does not exceed 15 degrees. The turbine inlet is imposed by tank pressure, being proposed to have the value 2.5 bar. The required power to support pumps consumed power should be around 280 kW. Being an upper stage, with functioning at a high altitude, the exit pressure was imposed as having 0.001 bar value. The working fluid temperature is, in this case, a variable that can be adjusted by modifying the mixture of the two fluids. The temperature will be limited to 1100 K for reasons related to the thermal and mechanical resistance of turbine materials. In table 4.3 are presented the turbine pre-design results:

Table 4.3 Turbine pre-design results

Inlet temperature (K)	**1100**	**Exit Mach Number**	**0.15**
Inlet pressure (bar)	**2.5**	**Inlet Base Radius (m)**	**0.09**
Rotational Speed (rpm)	**30850**	**Inlet Tip Radius (m)**	**0.107**
Power (kW)	**280**	**Exit Base Radius (m)**	**0.07**
Specific Work (kJ/kg)	**350**	**Exit Tip Radius (m)**	**0.127**
Pressure Ratio	**4**	**Mass flow rate (kg/s)**	**0.5**

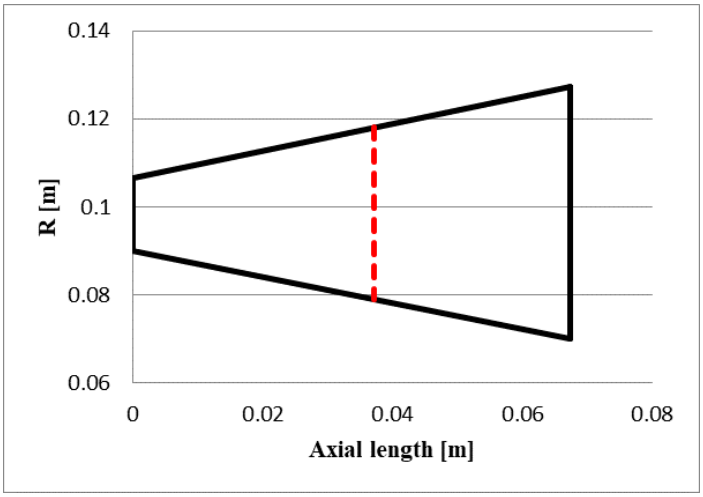

Fig. 4.2 Section through the turbine work channel

5. CONCLUSIONS

This paper provides an overview of the advantages of using methane fueled expander cycle upper stage engine, an overview of the analysis performed to parametrically study the performance characteristics, with particular focus on thrust chamber design and turbo-pumps feeding system general requirements.

A turbine pre-dimensioning calculation was performed, with the working channel defined based on the computation of the areas of the inlet and outlet sections. Under the conditions of a single turbine stage, its loading is high, which will result in low turbopump efficiency.

Single shaft, turbopump, methane fueled expander cycle engines is the optimal solution for hydrocarbon engines under investigation for future application.

In this paper, it was conducted a design procedure of a liquid oxygen liquid and of the liquid methane. Using the literature, a calculation and design methodology of the pump rotors was determined and using the Vista CPD software, the volute rotor assembly for each pump was pre-dimensioned. For the LOx pump, a 77.6mm rotor outlet diameter with a power output of 122kW was obtained and for the LCH4 pump the diameter of the rotor outlet was 120.1mm with a power output of 162kW

System performance and configuration studies indicate that a methane-fueled expander cycle is a viable candidate for upper stage propulsion.

ACKNOWLEDGEMENT

This work was carried out within "Nucleu" Program TURBOPROP, supported by the Romanian Minister of Research and Innovation, project number PN 19.05.01.02.

REFERENCES

[1] G. P. SUTTON, Rocket Propulsion Elements (Seventh Edition), by John Wiley & Sons, 2001, ISBN 0-471-32642-9
[2] M.J.L. Turner, Rocket and Spacecraft propulsion, Principles, Practice and New Developments (Second Edition), Springer, 2006, ISBN 3-540-22190-5
[3] D.K. Huzel, D.H. Huang, Modern Engineering for design of liquid-propellant rocket engines, AIAA, 1992, ISBN 1-56347-013-6
[4] David R. Lide, Handbook of Chemistry & Physics 1996-1997, 77th Edition; CPC Press Inc., 1996
[5] Source- Turbopump Systems for Liquid Rocket Engines NASA SP-8170
[6] Adhikari, Pradhumna & Budhathoki, Umesh & Raj Timilsina, Shiva & Manandhar, Saurav & Bajracharya, Tri. (2014). A Study on Developing Pico Propeller Turbine for Low Head Micro Hydropower Plants în Nepal. Journal of the Institute of Engineering. 9. 10.3126/jie.v9i1.10669.
[7] Research and Development of Rocket Turbopumps --- 35 Years în Retrospect published by Tohoku University Press, Sendai, în February, 2013. (http://www.frontier.phys.nagoya-u.ac.jp/jp/leading/files/Thubopump_of_Rocket_kamijo.pdf accesat 03.06.2019)
[8] Lampart, Piotr & Yershov, Sergiy & Rusanov, Andrey & Szymaniak, Mariusz. (2004). Tip leakage / main flow interaction în multi-stage HP turbines with short-height blading.
[9] Moustapha H. et al., Axial and Radial Turbines, Concepts ETI, Inc., 2003, ISBN0-933283-12-0
[10] M.J. Zhang, C.G. Gu, and Y.M. Miao, Numerical study of the internal flow field of a centrifugal impeller, *ASME Paper* 94-GT-357, 1994.
[11] K. Hillewaert and R.A. Van den Braembussche, Numerical simulation of impeller-volute interaction în centrifugal compressors, *ASME Journal of Turbomachinery*, vol. 121, pp.603-609, 1999.
[12] J. Gonzalez, J. Fernandez, E. Blanco, and C. Santolaria, Numerical simulation of the dynamic effects due to impellervolute interaction în a centrifugal pump, *ASME Journal of Fluids Engineering*, vol. 124, pp. 348-355, 2002.
[13] J. Gonzalez, J. Parrondo, C. Santolaria, and E. Blanco, Steady and unsteady forces for a centrifugal pump with impeller to tongue pump variation, *ASME Journal of Fluids Engineering*, vol. 128, pp. 454-462, 2006.
[14] J. Gonzalez, and C. Santolaria, Unsteady flow structure and global variables în a centrifugal pump, *ASME Journal of Fluids Engineering*, vol. 128, pp. 937-946, 2006.
[15] R. K. Byskov, C. B. Jacobsen, and N. Pedersen, Flow în a centrifugal pump impeller at design and off-design conditions- Part II: Large Eddy Simulations, *ASME Journal of Fluids Engineering*, vol. 125, pp. 73-83, 2003
[16] – Liquid Rocket Analysis-Development of Liquid Bi-Propellant Rocket Engine Design, Analysis and Optimization Tool, Master of Science Thesis, 2014, TUDelft
[17] Igor N. Nikischenko, Improving the performance of LOX/kerosene upper stage rocket engines, Propulsion and Power Research 2017; 6(3), 157-176
[18] Reuben Schuff, Matthew Maier, Oleg Sindly " Integrated Modeling for a Lox/Methane Expander Cycle Engine: Focusing on Regenerative Cooling Jacket Design", AIAA 2006-4534
[19] Marco Leonardi, Francesco Nasuti "Basic Analysis of a LOX/Methane Expander Bleed Engine", DOI: 10.13009/EUCASS2017-332

ANALYSIS OF THE VOLUMETRIC EFFICIENCY OF THE BLOWER ROTORS WITH LOBES

Teodor STĂNESCU[1], Gabriel-Petre BADEA[1], Nicușor-Daniel STAN[1], Elena PRESURĂ-CHIRILESCU[1]

ABSTRACT: Within this article were studied 3 types of rotors based on different profile curves. For these, the 2D model of the profile was established starting from the parametric relations that describe the curves, subsequent by defining the computational relations of the volumetric machine parameters, a comparison criterion was established following which the most efficient type of rotor was identified.

Keywords: lobe blower, lobe blower profile, involute, cycloide, hypocycloide.

NOMENCLATURE

D_c	Housing diameter	η_m	Mechanical efficency
R_c	Housing radius	Q_r	Volumetric machine real flow
L_r	Rotor length	p_a	Suction pressure
L_c	Housing length	p_r	Discharge pressure
n	Electric engine speed	Δp	Differential pressure
A_c	Housing diameter area		
A_r	Rotor area	M_t	Moment of torsion[5]
V_g	Displacement / Engine displacement	P	Power
Q_{1rotor}	Theoretical flow provided by a single rotor	θ	Rotation angle
Q_t	Volumetric machine theoretical flow	j_a	Axial clearance
η_v	Volumetric efficency	j_r	Radial clearance

1. INTRODUCTION

Lobe blowers are volumetric compression machines used in a variety of industries, including cellulose and paper, chemicals, food, pharmaceuticals and biotechnology. They are popular because they offer high efficiencies, reliability, corrosion resistance and are very easy to maintain.

These machines can be classified in terms of number of lobes, thus there are pumps with two,three or four lobes, with straight or helical lobes.

The shape of the lobe and the analysis of the rotors gearing of the blowers / compressors are the basis of many scientific works. Mimmi [1] used in his work a mathematical model for optimizing the parameters of the lobes. Wang [2] designed a lobe consisting of five circle arches with improved sealing efficiency, and Chiu [3] developed a new profile using elliptic curves and then compared the performances with those of traditional profiles. Hwang [4-5] proposed a new shape of the lobe, where it investigated how high volumetric efficiency and better sealing performance can be achieved. The same problem was studied by Tong and Yang [6-8][18]. With the development of fluid dynamics (CFD), a growing number of researchers have focused on numerical analysis of volumetric machines, such as the screw compressor and the lobe pump. Regarding the screw compressor, Stosic [9] described the generation of rotors based on the method of generating the racks. Kovacevic [10, 11] developed a static model to simulate the flow through the volumetric voids of the machines.

[5] Romanian Research and Development Institute for Gas Turbines COMOTI, Bucharest, Romania

Li [12] investigated pressure variations using a two-dimensional turbulence model. Huang [13] used the κ-ε model to simulate a three-lobed pump and compared the results obtained using the speciality literature[18].
In this article, 3 types of rotors based on profiles formed from different curves are studied, and for the most favorable constructive model, a CFD analysis was performed.

2. ROTOR PROFILE

2.1. HYPOCYCLOIDAL AND EPICYCLOIDAL PROFILE

In order to determine the shape of the rotors (lobes profile), several types of curves will be analyzed from a functional and technological point of view, which can describe the rotor profile.

In geometry, a hypocycloid is a plane curve drawn by a point fixed on a circle that rolls inside another larger circle (figure 1), and an epicycloid is a plane curve drawn by a point fixed on a circle that rolls on the outside of another larger circle (figure 2). [14]

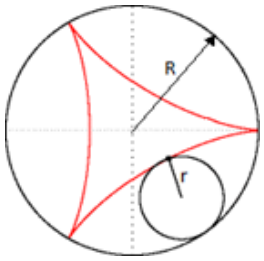

Fig. 1 Hypocycloidal curve

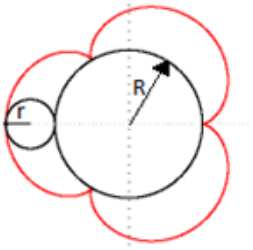

Fig. 2 Epicycloidalcurve

A blower rotor with lobes can have the profile formed by 2 curves:

- the head of the tooth is formed from a portion of the epicycloid curve;
- the base of the tooth from a portion of the hypocycloid curve.

Such a lobed rotor in which the profile consists of the hypocycloid and epicycloid curves is shown in Figure 3.

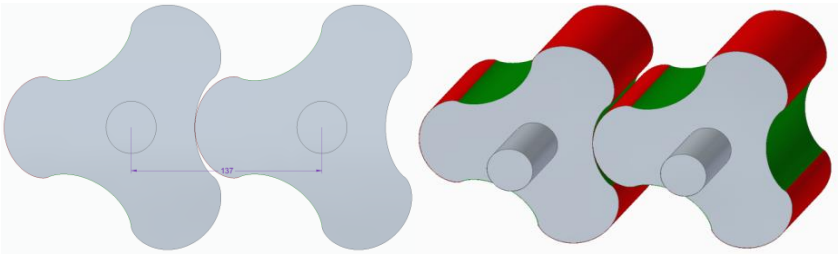

Fig. 3 Rotors with 3 lobes (having hypocycloidal and epicycloidal profile)

2.2. INVOLUTE PROFILE

Involute (Figure 4) is the curve described by a point M belonging to a straight line Δ which rolls without sliding on a circle of radius r called a base circle. [16]

The rotor with involute profile can be likened to a gear wheel with a very small number of teeth. According to the gearing theory of gear wheels, for the standard pressure angle of 20 °, the minimum number of teethes on the gear is 17. If this number is smaller, the phenomenon of underfeeding at the base of the tooth appears. This problem is solved by constructive upgrades of the tip of the tooth and the gap between the lobes.

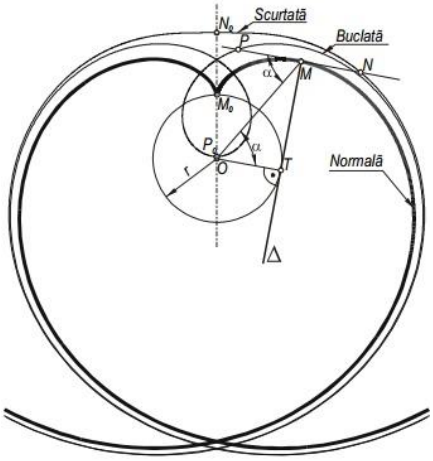

Fig. 4 Generating the involute profile

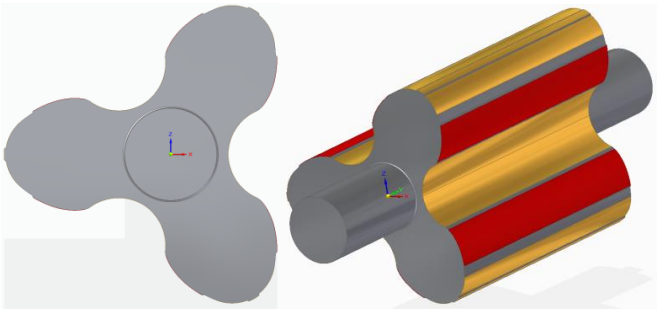

Fig. 5 Rotors with 3 lobes (with involute profile and circle arche)

Unlike the constructive variant of the rotor made from the hypocycloid and epicycloid profile, where the clearance between the rotors will be kept constant at a complete rotation of the shaft, in the case of the rotor with involute profile and circle arches the clearance between the 2 rotors will vary, but not much , ± 0.1 mm.

2.3. CYCLOIDAL PROFILE

A cycloid is a curve drawn by a fixed point on a circle that rolls on a straight line. [17]

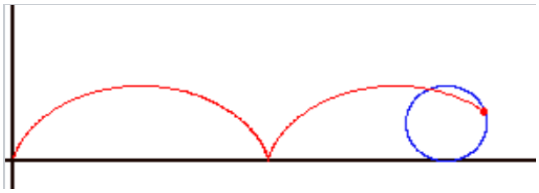

Fig. 6 Cycloid generated by a rolling circle [4]

The cycloid equations. The cycloid passing through origin, created by a circle with radius r, is formed by the points (x, y) with:

$$x = r \cdot (t - \sin(t)) \quad (1)$$

$$y = r \cdot (1 - \cos(t)) \quad (2)$$

where t is a real parameter, equal to the angle at which the generator circle is rotated.

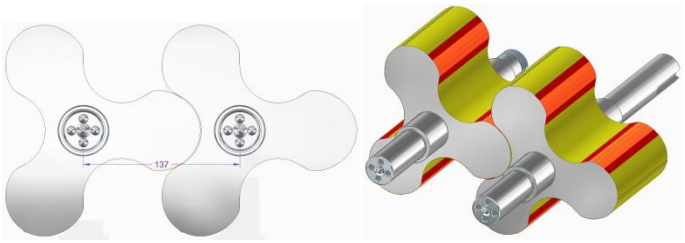

Fig. 7 Rotors with 3 lobes (which have cycloid, straight lines and circle arches)

Figure 7 shows from a constructive point of view blower / compressor rotors with 3 lobes that have a profile consisting of cycloid (orange area), straight line (red area) and circle arches (yellow area).

3. MATHEMATICAL CALCULATION OF BLOWER PARAMETERS

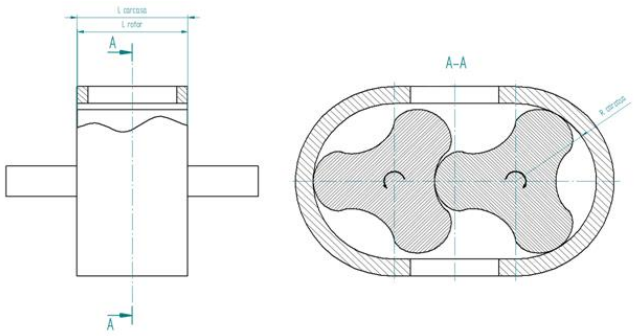

Fig. 8 Rotors with 3 lobes (that have cycloid profile, straight lines and circle arches)

Figure 8 shows a simplified diagram of the assembly between 2 rotors with lobes and housing, in which:

$$D_c[mm] = 2 \cdot R_c[mm] \tag{3}$$

where R_c is chosen as the value from the center axis to the farthest point on the epicycloid portion assembled with the clearance between the lobe and the housing (generally the clearancehas values between 0.05 and 0.25 mm).

$$L_c[mm] = L_r[mm] - j_a[mm] \tag{4}$$

in which:

- j_a is the axial clearance between the housing and the rotor (generally the clearance has values between 0.2 and 0.7)

By imposing a speed of rotation for both rotors one can determine the theoretical flow, this being directly proportional to the displacement of the volumetric machine, displacement that can be defined as the total volume of fluid that travels the machine at a complete rotation of the engine shaft.

$$V_g[cm^3] = (A_c[mm^2] - A_r[mm^2]) \cdot 2 \cdot L_r[mm] \cdot 10^{-3} \tag{5}$$

where:

$$A_c[mm^2] = \pi \cdot \frac{D_c^2[mm]}{4} \tag{6}$$

$$Q_{1rotor}\left[\frac{m^3}{min}\right] = (A_c[mm^2]\cdot L_c[mm] - A_r[mm^2]\cdot L_r[mm])\cdot n\left[\frac{rot}{min}\right]\cdot 10^{-9} \quad (7)$$

$$Q_t\left[\frac{m^3}{h}\right] = Q_{1rotor}\left[\frac{m^3}{min}\right]\cdot 2\cdot 60 \quad (8)$$

$$Q_r\left[\frac{m^3}{h}\right] = Q_t\left[\frac{m^3}{h}\right]\cdot \eta_v[\%] \quad (9)$$

The moment of torque can be approximated by a semi-empirical relation:

$$M_t[N\cdot m] = \frac{V_g[cm^3]\cdot \Delta p[bar]\cdot 1{,}59155}{\eta_m[\%]} \quad (10)$$

in which:

$$\Delta p[bar] = p_r[bar\ absolut] - p_a[bar\ absolut] \quad (11)$$

$$P[kW] = \frac{M_t[N\cdot m]\cdot \pi\cdot n\left[\frac{rot}{min}\right]\cdot 10^{-3}}{30} \quad (12)$$

4. COMPARISON BETWEEN LOBE PROFILES

In order to evaluate the 3 types of rotors presented above, a comparative calculation can be made using the computational relationships 3… 12.

It is necessary:

- Rotor length $L_r = 124{,}7\ mm$;
- Speed $n = 2.900\,\frac{rot}{min}$;
- Pressure discharge $p_r = 1{,}55\ bar\ absolut$;
- Volume efficiency $\eta_v = 75\ \%$;
- Mechanical efficiency $\eta_m = 90\ \%$;
- Clearances $j_a = j_r = 0{,}15\ mm$.

Table 1. Different rotor profile calculated parameters

Parameters	Hypocycloid + epicycloid	Involute	Cycloid
$D_c\ [mm]$	182,66	203,72	206,1
$R_c\ [mm]$	91,33	101,86	103,05
$A_c[mm^2]$	26.204,55	32.595,47	33.361,52
$A_r[mm^2]$	15.522,78	15.464,69	15.807,87
$V_g[cm^3]$	2.664,03	4.272,42	4.377,88
$Q_t\left[\frac{m^3}{h}\right]$	466,28	746,8	765,23
$Q_r\left[\frac{m^3}{h}\right]$	349,71	560,1	573,93
$M_t[N\cdot m]$	25,911	41,554	42,58
$P\ [kW]$	7,869	12,619	12,931

It can be noticed from the table above that from a functional point of view the profile formed by the hypocycloid and epicycloid is the most ineffective, having a very low displacement. Also, from a functional

point of view, the functional characteristics of the other 2 profiles (involute and cycloid) are close, the differences between them being maximum 3%.

From a technological point of view, the profile formed by the involute requires a careful processing on a much larger surface than the profile formed by the cycloid.

From the point of view of control dimensions, the profile formed with the cycloid has the advantage of a straight reference surface, so that exact dimensions of dimensional control can be indicated.

5. CONCLUSIONS

From the analysis of the different curves that can describe the rotor profile, it was concluded that the profile formed by the hypocycloid and the epicycloid is the most ineffective in terms of the volume of fluid conveyed at a complete rotation of the shaft. The profiles formed from involute + circle arches and cycloid + straight lines+ circle arches have close efficiency, differences between them being maximum 3%, and from the technological point of view the profile that has a cycloid component have more advantages.

Due to the fact that lobe blowers did not reached the maximum point of development, research on this topic can continue.

REFERENCES

[1] G. Mimmi, P. Pennacchi, G. Mimmi, Analytical model of a particular type of positive displacement blower, ARCHIVE Proc. Institution Mech. Eng. Part C J. Mech. Eng. Sci. 213 (5) (1999) 517e526.
[2] P.Y. Wang, Z.H. Fong, H.S. Fang, Design constraints of five-arc Roots vacuum pumps, Proc. Institution Mech. Eng. Part C 216 (2) (2002) 225e234.
[3] C.F. Hsieh, A new curve for application to the rotor profile of rotary lobe pumps, Mech. Mach. Theory 87 (2015) 70e81.
[4] Y.W. Hwang, C.F. Hsieh, Study on high volumetric efficiency of the Roots rotor profile with variable trochoid ratio, Proc. Institution Mech. Eng. Part C J. Mech. Eng. Sci. 220 (9) (2006) 1375e1384.
[5] C.F. Hsieh, Y.W. Hwang, Study on the high-sealing of Roots rotor with variable trochoid ratio, J. Mech. Des. 129 (12) (2007) 1278e1284.
[6] S.H. Tong, D.C.H. Yang, On the generation of new lobe pumps for higher pumping flow rate, Mech. Mach. Theory 35 (35) (2000) 997e1012.
[7] D.C.H. Yang, S.H. Tong, The specific flow rate of deviation function based lobe pumps - derivation and analysis, Mech. Mach. Theory 37 (10) (2002) 1025e1042.
[8] S.H. Tong, D.C.H. Yang, Rotor profiles synthesis for lobe pumps with given flow rate functions, J. Mech. Des. 127 (2) (2005) 287e294.
[9] N. Stosic, I.K. Smith, A. Kovacevic, et al., Geometry of screw compressor rotors and their tools, J. Zhejiang University-SCIENCE A 12 (4) (2011) 310e326.
[10] A. Kovacevic, I.K. Smith, The influence of rotor deflection upon screw compressor performance, Vdi Berichte 1715 (2002) 17e28.
[11] Li Y B, Jia K, Meng Q W, et al. Flow simulation of the effects of pressure angle to lobe pump rotor meshing characteristics. 6th international conference on blowers and fans with compressors and wind turbines, materials science and engineering, 2013, 52(3):032022.
[12] Z.F. Huang, Z.X. Liu, Numerical study of a positive displacement blower, ARCHIVE Proc. Institution Mech. Eng. Part C J. Mech. Eng. Sci. 223 (10) (2009) 2309e2316.
[13] Florian MENTER,J. C. FERREIRA,T. ESCH,B. KONNO, "The SST Turbulence Model with Improved Wall Treatment for Heat Transfer Predictions in Gas Turbines", Proceedings of the International Gas Turbine Congress 2003 Tokyo November 2-7, 2003
[14] https://en.wikipedia.org/wiki/Hypocycloid– Accessed on 08.10.2019
[15] https://en.wikipedia.org/wiki/Epicycloid– Accessed on 08.10.2019
[16] https://math.wikia.org/ro/wiki/Evolvent – Accessed on 08.10.2019
[17] https://en.wikipedia.org/wiki/Cycloid – Accessed on 08.10.2019
[18] T.Stănescu,I.Mălăel,D.Rădulescu, Modelarea şi simularea unei maşini de comprimare volumetrică a aerului cu pistoane rotative cu 3 lobi. Cercetări privind influența rezonatorului Helmholtz asupra zgomotului produs de mașină., PN 19.05.02.01-3

CROSS-FLOW HEAT TRANSFER WITH APPLICATIONS IN TURBINE BLADES COOLING

Mădălin DOMBROVSCHI[1]

ABSTRACT: In this paper, the heat transfer phenomenon in a cross-flow it will be discussed. In the first part of the paper, the theory behind the paper will be presented with the most important physical parameters described, then a presentation of the numerical calculations and the geometry follows. The paper ends with a presentation of the results in a graphical way and some conclusions. After the results were discussed, the final conclusion is that the results are encouraging and the simulations seem good, an experimental analyze is require to see if the real world the results will be the same.

KEYWORDS: heat transfer, CFD, CFX, cross-flow

1. INTRODUCTION

It is well known that for a turbine to produce a bigger power, the temperature in front of the turbine has to be higher. All along the years, a lot of methods have been developed for increasing high temperature resistance, such as introducing new alloys of material, or developing some cooling techniques, for example the film cooling, which is a method which collects a small percentage of the compressor air, guides it through the internal channels in the turbine blades, and discharges it through small holes in the blade walls. The discharged air is forming a thin blanket around the turbine blade, that keeps the turbine blade surface temperature lower.

This paper focuses on the heat transfer methodology for a cross-flow, which is the exact type of flow that exists in the cooling of the turbine blades. In this paper, no specific turbine blade geometry was used.
It is very important to understand that this paper will be followed by an experimental study, that being the main reason why the numerical simulation was made on similar geometry to a turbine blade. The results of the upcoming experiment will be compared with the results of the numerical calculation and this comparison will be presented in a future paper.

2. THEORY BEHIND THE PAPER

The heat transfer calculation begins with the calculation of the Reynolds number. The reason for that is to determinate what kind of flow it, is so the Nusselt number may be determined, which is one of the quantities that is needed in the calculation of the heat-transfer coefficient.
The problem itself is described as follows. In a medium of a flow that has as a working fluid air ideal gas with the temperature equals to $1000℃$ and a velocity of $10\,m/s$ comes across a rectangular plate that has inside it a number of cooling tubes through which an air ideal gas with the temperature of $600℃$ and a velocity of $10\,m/s$ passes.

The heat transfer will be produced in this order: first, forced convection occurs between the hot air and the wall, then heat conduction will appear inside the wall, and then internal forced convection. The last one occurs because the fluid is forced to flow in a desired direction.

One may have probably noticed that most fluids, especially liquids, are transported in circular pipes. This is because pipes with a circular cross section can withstand large pressure differences between the inside and the outside without undergoing significant distortion. For a fixed surface area, the circular tube gives the most heat transfer for the least pressure drop, which explains the overwhelming popularity of circular tubes in

[1] Romanian Research and Development Institute for Gas Turbines COMOTI, Bucharest, Romania

heat transfer equipment [1]. This paper will focus on explaining the internal forced flow as much as possible. Due to its complexity the problem presented earlier can't be solved analytically.

For the internal flow of the cooling air, it is highly important to understand two physical parameters, which are the average velocity and temperature, so the next paragraphs will be dedicated to explaining these parameters. In the external flow, the free-stream velocity served as a convenient reference velocity for use in the evaluation of the Reynolds number and the friction coefficient. In the internal flow, there is no free stream and thus an alternative is needed. The fluid velocity in a tube changes from zero at the surface because of the no-slip condition, to a maximum at the tube center. Therefore, it is convenient to work with an average or mean velocity, which remains constant for incompressible flow when the cross-sectional area of the tube is constant. [1]

The value of the average velocity at some streamwise cross section is determined from the requirement that the conservation of mass principle be satisfied. [2]

$$\dot{m} = \rho V_{avg} A_c = \int_{A_c} \rho u(r) d\, A_c \tag{1}$$

Then, the average velocity for incompressible flow in a circular pipe of radius R is expressed as

$$V_{avg} = \frac{\int_{A_c} \rho u(r) d\, A_c}{\rho A_c} = \frac{\int_0^R \rho u(r) 2\pi r\, d\, r}{\rho \pi R^2} = \frac{2}{R^2} \int_0^R u(r) r\, dr \tag{2}$$

where, A_c is the cross-sectional area, ρ is the density of the fluid, $\dot{m}$ is the mass flow, R is the radius of the circular pipe and $u(r)$ is the velocity profile.

Therefore, if the flow rate or the velocity profile are known, the average velocity can be determined easily [2]. When a fluid is heated or cooled as it flows through a tube, the temperature of the fluid at any cross-section changes from the temperature at the surface of the wall to some maximum (or minimum in the case of heating) at the tube center. In fluid flow, it is convenient to work with an average or mean temperature, which remains constant at a cross section. Unlike the mean velocity, the mean temperature changes in the flow direction whenever the fluid is heated or cooled. [1]

The value of the mean temperature is determined from the requirement that the conservation of energy principle be satisfied. That is, the energy transported by the fluid through a cross section in actual flow must be equal to the energy that would be transported through the same cross section if the fluid were at a constant temperature.

$$T_m = \frac{\int_{\dot{m}} c_p T(r) \delta \dot{m}}{\dot{m} c_p} \tag{3}$$

3. NUMERICAL CALCULATION

Before the numerical simulation starts, an analytical calculation is needed for the determination of the velocity field. This calculation was made using equation 1, imposing the mass flow of the coolant to vary between 0.4-1.8% of the hot air mass flow. The reason for that is the similarity between this case and the case of a turbine blade cooling. [3] The results of the analytical calculation can be found in table 1.

Table 1. Results of the numerical calculation

Hot air mass flow: 0.0031331 [kg/s]		
Percentage [%]	**Coolant mass flow [kg/s]**	**Speed [m/s]**
0.4	0.001253	10.97538
0.5	0.001567	13.71922
0.6	0.00188	16.46307
0.7	0.002193	19.20691
0.8	0.002506	21.95076
0.9	0.00282	24.6946
1	0.003133	27.43845
…	…	…
1.8	0.00564	49.3892

As it can be seen in table 1, the velocity varies between 10 to 50m/s, so in the numerical calculation that will come the velocity will be the one presented in table 1. As it was mentioned before, the problem in this paper wants to be very similar with a cooling turbine blade heat transfer problem, so an appropriate geometry is in need. Figure 1 shows the geometry with one, three and five cooling tubes.

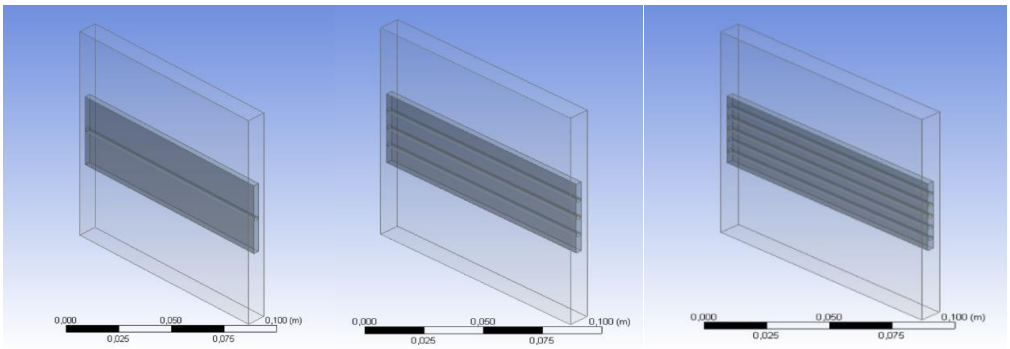

Fig. 1 Geometry of the problem, with one, three and five cooling tubes

The numerical simulation was carried out using ANSYS CFX for the simulation and the ANSYS workbench mesh generator for the grid generation. The domains principal boundaries can be seen in figure 2. As shown, the flow from the inlet of the hot domain and the flow from the inlet of the cold domain are in a cross flow. The conditions at nominal input are:

Inlet conditions:

- Static temperature for hot domain: 1273.15 [K]
- Static temperature for cold domain, for each tube: 873.15 [K]
- Velocity of the hot fluid: 10 [m/s]
- Velocity of the cooling fluid, for each tube: 10 [m/s]

Outlet conditions:

- Relative pressure for the outlet of each tube, 0 [Pa]
- Relative pressure for the outlet of the hot domain, 0 [Pa]

Wall conditions:

- No slip walls
- Adiabatic wall

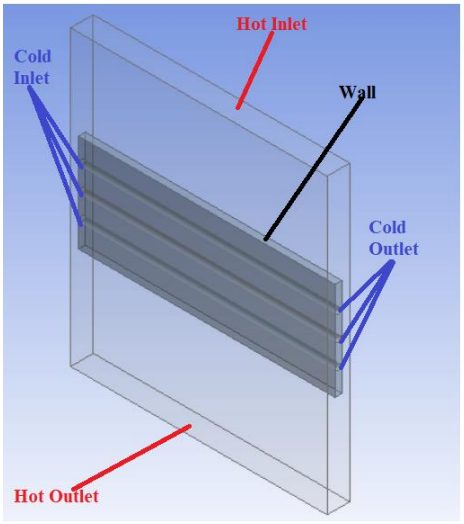

Fig. 2 The boundaries of the calculation domain for the three cooling tubes geometry

The material chosen for the wall domain is Nickel, with the proprieties from ANSYS material library. The thermal radiation was neglected and the simulations were conducted in stationary regime. A number of 1250 iterations was performed for each one of this cases, for the convergence criteria a value of 10^{-15} was imposed for the residual target.

The hot domain represents the numerical domain with a static temperature of 1273.15K imposed for the entire volume, while the cold domain represents each cooling tube and it has a static temperature of 873.15K imposed for the entire volume. The domain of interest is represented by the wall domain, which is a simple representation of the turbine blade, so its surface temperature would represent the turbine blade surface temperature.

A number of 9 numerical cases have been simulated for each geometry. More cases have been simulated to allow to change the velocity in the cold domain, varying it from 10 m/s all the way to 50 m/s, while the hot domain mass flow remains constant. This change is also a similarity with the cooling of the turbine blades, because in that case the mass flow that enters the turbine blade to cool it can be controlled while the mass flow of the gases that come from the combustion chamber cannot be controlled so easily. In figure 3, 4 and 5 it is presented the results of the 3 tubes case but with different speed for the cooling fluid.

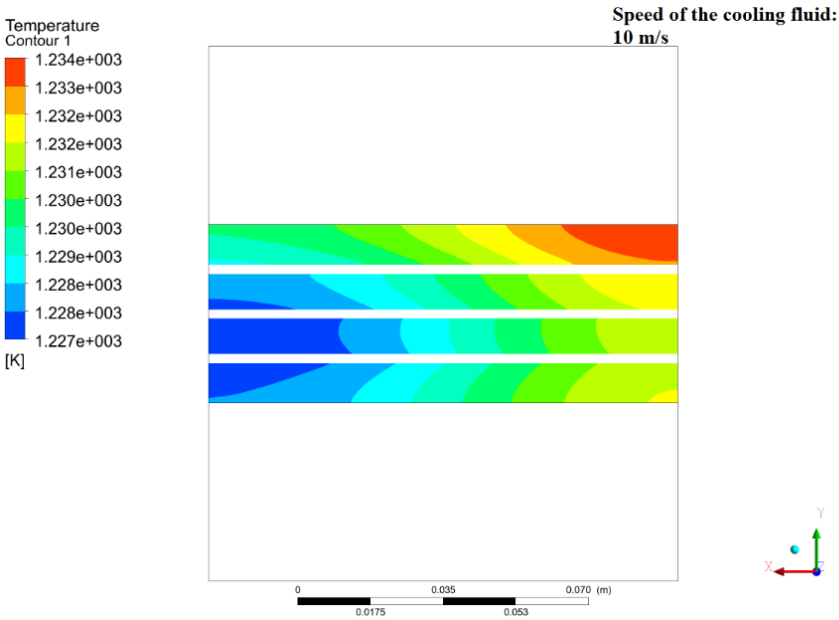

Fig.3 The variation of the wall temperature for the 3 tubes case with the speed of 10 m/s for the cooling fluid

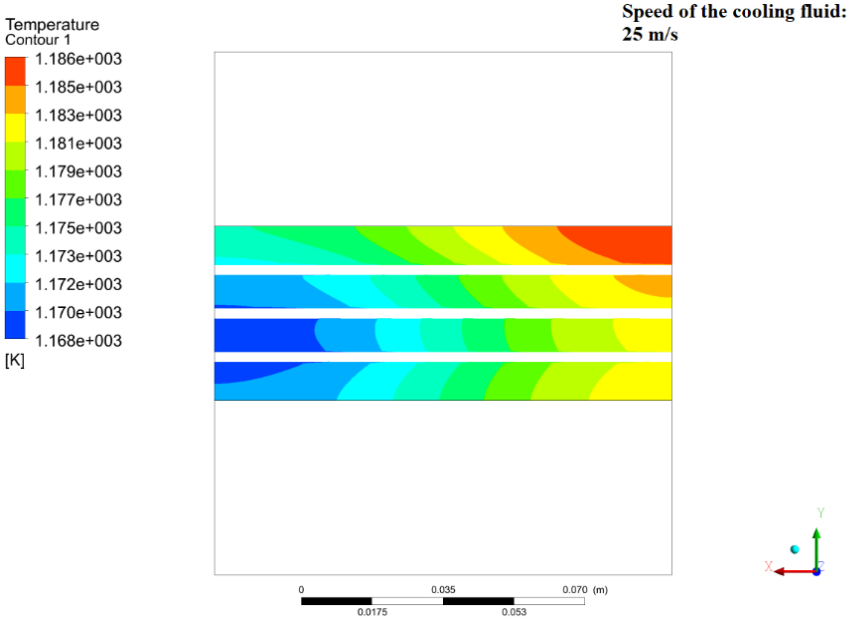

Fig.4 The variation of the wall temperature for the 3 tubes case with the speed of 25 m/s for the cooling fluid

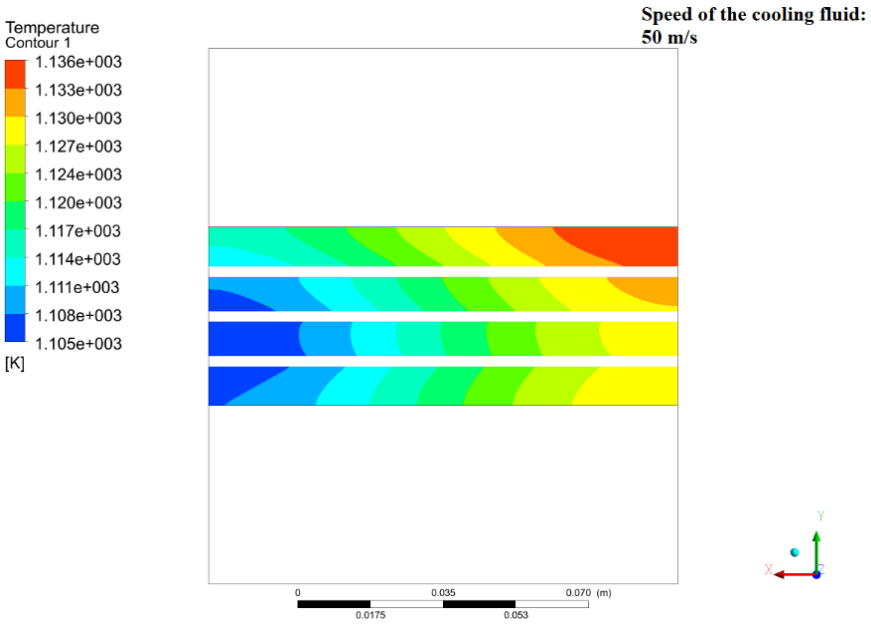

Fig.5 The variation of the wall temperature for the 3 tubes case with the speed of 50 m/s for the cooling fluid

For a even better observation of the differences, for the same cold air speed, the results for the 3 geometrical configurations are presented in figure 6, 7 and 8.

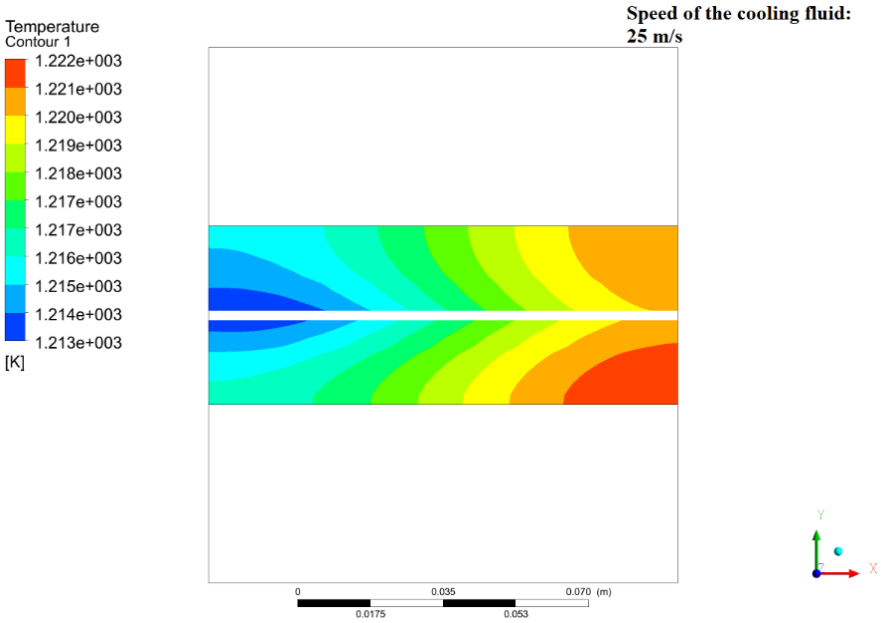

Fig.6 The variation of the wall temperature for the 1 tube case with the speed of 25m/s for the cooling fluid

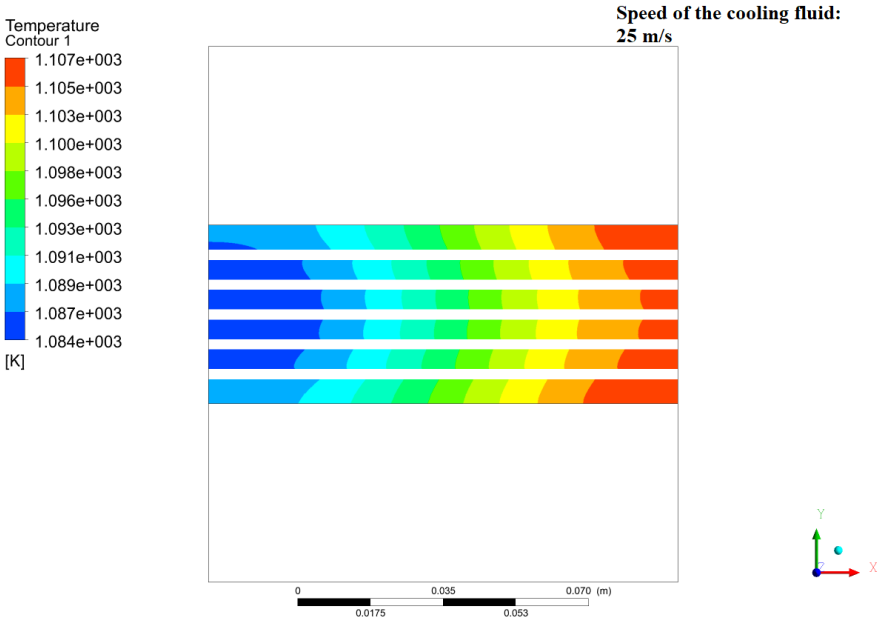

Fig.7 The variation of the wall temperature for the 5 tubes case with the speed of 25m/s for the cooling fluid

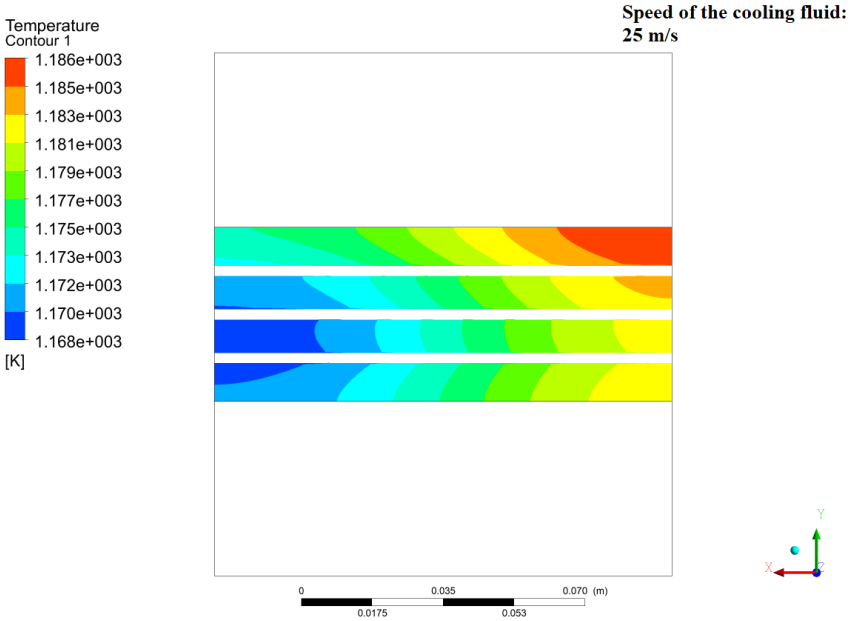

Fig.8 The variation of the wall temperature for the 3 tubes case with the speed of 25m/s for the cooling fluid

4. RESULTS

As it was said before, it was solved a number of nine numerical cases and the interest data were the maximum, medium and minimum temperature of the wall. In figure 9 it can be seen a graphical illustration of the wall temperature variation based on the cooling fluid velocity.

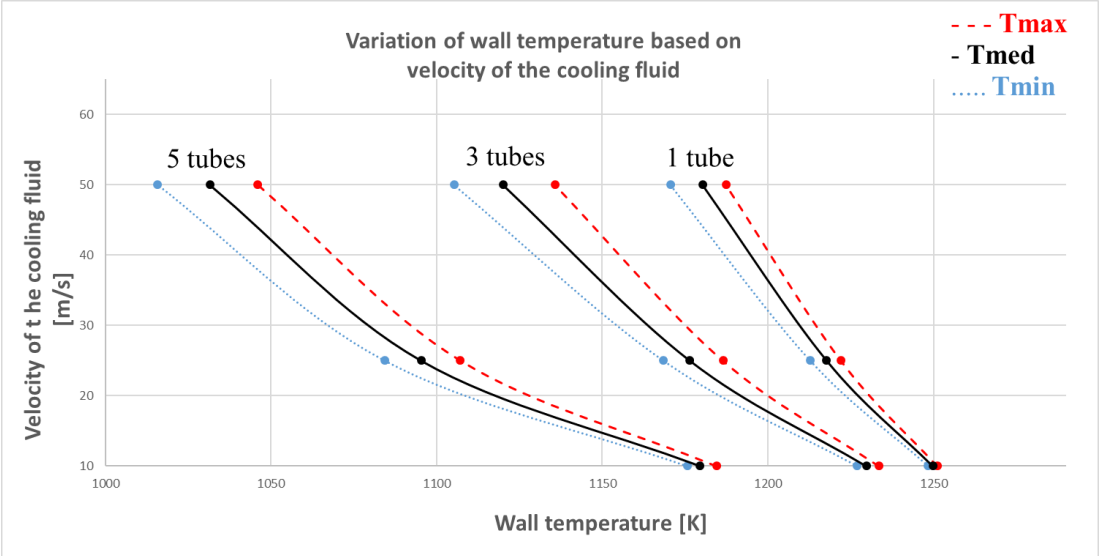

Fig. 9 Variation of the wall temperature based on the velocity of the cooling fluid

As it can be observed, the lowest temperature is acquired when be difference between the cooling fluid velocity and the hotter fluid velocity is the biggest, so if the hot fluid velocity remains constant at 10 m/s the lowest temperature is acquired when the velocity of the cooling fluid is the 50 m/s. Also, based on the figure 7, the number of the cooling tubes can be determined for a desired wall temperature and for a known velocity of the cooling fluid.

These results are encouraging, it can be observed that even with one tube the temperature dropped from 1273.15 K to 1251.18 K in the simplest case possible, meaning one tube with a velocity of 10 m/s. That temperature drops of 20 degrees in the worst-case scenario can make a difference in a turbine blade case. Since the case presented in this paper is a similarity of the turbine blades cooling, a graphical illustration of the wall temperature based on the percentage of the cooling fluid mass flow out of hot fluid mass flow must be done.

The reason for that is that mostly of the turbomachinery work with the mass flow parameter, so a correlation between this two, temperature and mass flow, is well received. Unfortunately, this graphical illustration can't be created because the values are too close to each other and it would be impossible to interpret them. Another similarity that can be presented is the heat of the case presented in this paper. It is well known that the heat is the energy that can be transferred from an object to another. So, this parameter is very important in all kind of heat transfer applications. A graphical illustration is presented in figure 10.

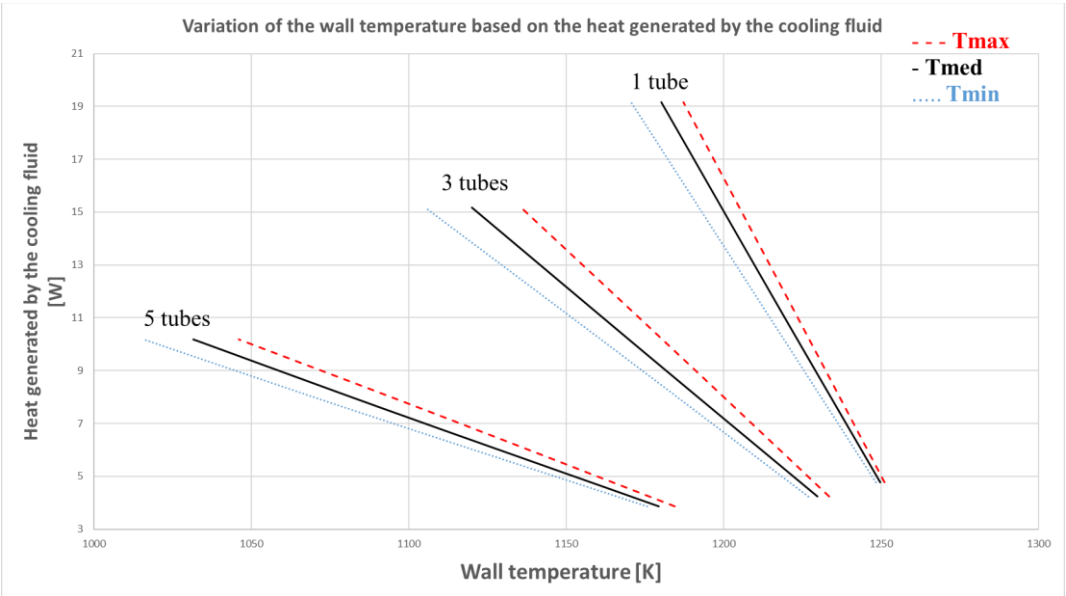

Fig. 10 Variation of the wall temperature based on the heat generated by the cooling fluid

From figure 10, it can be observed that the results of the simulations are correct. As it can be seen, the highest temperature and heat is obtained in the case with only one cooling tube and the lowest is acquired in the 5 tubes case. From this figure it can be predicted how the wall temperature will behave for a case with 4 or 2 cooling tubes, also if a lower value of the generated heat is obtained using another fluid, another than air, it would be interesting to study this problem to see if it's more viable using another fluid instead of using air from the compressor.

5. CONCLUSIONS

In this paper was presented a method of cooling a surface that is exposed to a flow of a very high temperature fluid was presented and analyzed using the numerical simulations. The graphical illustration was obtained changing one input value multiple times for three different geometries. For future work, as it was said before, a physical experiment will follow trying to obtain similar results, or with an error of maximum 5%. If this error will be achieved or lowered, a similar experiment will begin, but this time instead of the simplified geometry a turbine blade geometry will be introduced. An experimental stand will be created to confirm this methodology using the same inputs that were presented in this paper, temperature, velocity etc. Then, a cooled turbine blade will be designed using a CAD program then it will be simulated using a numerical simulation program then a physical geometry will be created and tested in the same way. The experiment will be made using a hot source that will produce a flux of a desire temperature on the desired geometry and the cooling will be produce using pipes that will have installed on them pressure, temperature and mass flow sensors so these 3 parameters can be controlled from distance.
As it was said before, the mass flow of the cold domain in the nominal condition represents 0.63% of the mass flow of the hot domain, this thing is also encouraging to see such significant drop of temperature with such a small percentage of the mass flow.

REFERENCES

[1] Yunus A. Cengel, Afshin J. Ghajar, ,, Heat and Mass Transfer: Fundamentals and Applications, 5th Edition", McGraw-Hill Science/Engineering/Math, United States of America, 2014, ISBN: 978-007-339-818-1

[2] J.P. Holman, „Heat Transfer tenth Edition", McGraw-Hill Science/Engineering/Math, United States of America, 2009, ISBN: 978-007-352-936-3

[3] Daniel Crunțeanu, Ioan Manole, „CALCULUL MOTOARELOR AEROREACTOARE "- octombrie 2016, editura Politehnica Press, ISBN 978-606-515-714-9

ADDITIVE MANUFACTURING APPLICATION FOR A TURBOPUMP ROTOR

Cristian DOBROMIRESCU[1], Valeriu VILAG[1]

ABSTRACT: This paper presents application of the additive manufacturing of a rotor turbine, used for liquid fuel rocket turbopumps. The design process is composed of material strength optimization, dimensional tolerances and manufacturing requirements definitions of the turbine rotor. By coupling the obtained turbine design with a metal additive manufacturing process, the paper studies and presents the technological capabilities of the additive manufacturing technology available, and compares them to the design imposed technological requirements.

KEYWORDS: turbine, design, additive manufacturing, rotor, turbopump, blade.

1. INTRODUCTION

Turbopumps are devices crucial to liquid fuel rocket engines, allowing increased combustion chamber pressure without raising the fuel and oxidizer tanks pressures. The turbopump extracts the necessary work for powering the fuel and oxidizer pumps by coupling them with one or more turbines. The work provided by the turbines is extracted from a flow of gas, either heated gaseous fuel or burnt gases. They present many challenges from a manufacturing standpoint, so the additive manufacturing technology poses a great advantage for this type of parts.

The state of the art, in Romania, regarding aerospace applications of 3D printing is very scarce. This paper focuses on the optimization and the possibilities that the technology offers to the aerospace domain, and tackles a more technical and original concept-oriented approach, thus thermodynamic design is not discussed, as in other similar publications. The subjects presented heavily based on original concepts and come as a first step in the field of aerospace.

Based on the fact that the technology's concept is quite original and new, it can offer solid advantages and alternatives for the manufacturing industry, so the exploration of the possibilities the technology is very important.

The 3D technology is not the only technology available that can manufacture the geometries presented, but seems to offer a great advantage regarding the difficulty, cost and time efficiency of the manufacturing process.

2. TURBINE DESIGN

2.1. Design and stress optimization

For the material strength and optimization of the turbine rotor a CAD model of an axial turbine rotor was used. This rotor was chosen, from an internal database owned by COMOTI, not accessible to the public. The choice comes from taking into consideration the dimensions of the 3D printing enclosure and the quantity of metal powder required for the printing job. The aforementioned CAD model is presented in Fig. 1.

[1] National Research and Development Institute for Gas Turbines COMOTI, Bucharest, Romania

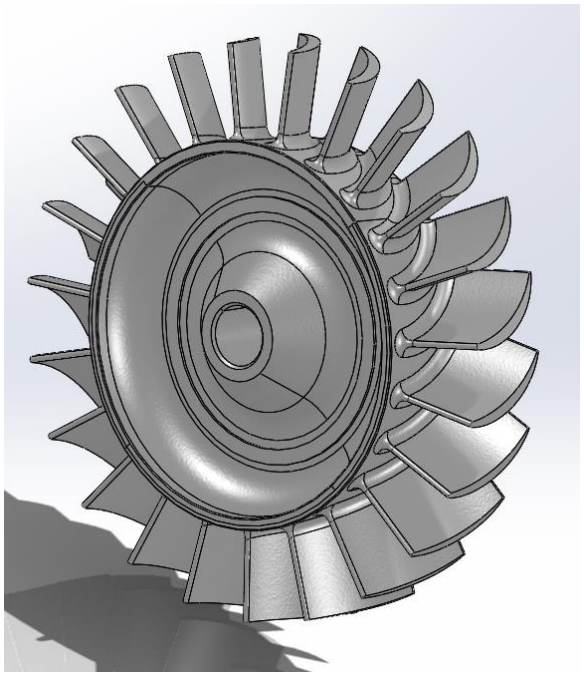

Fig. 1 Initial rotor CAD model without optimization

The mass of the model is calculated using CAD Solidworks 2018 with the material density given by the wanted material (EOS – MP1 CoCr), and the value is 368.59 g.

For mass reduction a material removal method was proposed so that the thermodynamic role of the rotor is not affected. A detail is presented in Fig. 2 showing two blades side by side, one emptied and one full of material, as well as defining the method of extracting material.

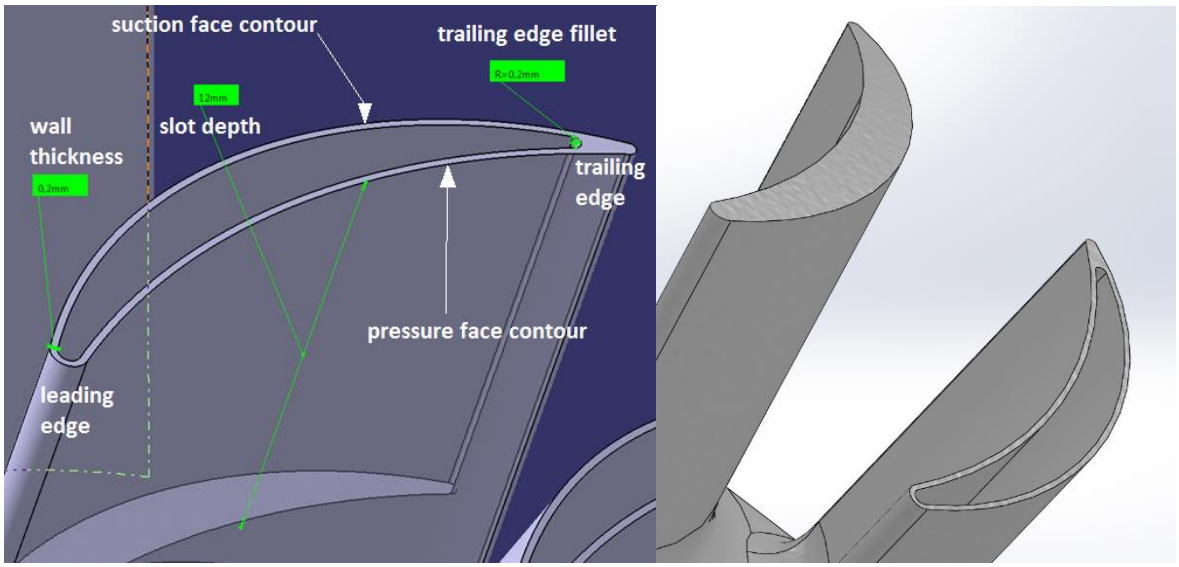

Fig. 2 Detail presenting the full and emptied blades and a definition of the slot

The mass reduction was achieved by creating a slot inside the blade. A sketch was drawn at the tip of the blade and then used to remove material, in radial direction, for a certain depth. The defining sketch of the slot was created by offsetting the blade tip outer contour with another value, named the wall thickness, applied to all the sides of the blade contours except the trailing edge of the blade. At the trailing edge there was defined a fillet between the pressure and suction surfaces contours of the sketch. The wall thickness and slot depth were considered as parameters for optimization and the results of interest were mass and centrifugal stresses and strains.

For the walls thickness, the following values were considered: 0.2 mm, 0.3 mm, 0.4 mm, while for the slot depth the considered values were: 9 mm, 11 mm, 13 mm, 15 mm. That means that there are 15 combinations to study each requiring its own CAD model. These combinations are shown in Table 1.

Table 1. The results of mass, maximum stress and maximum strain calculated

No.	Wall thickness [mm]	Slot depth [mm]	Total mass [g]	Maximum Von Mises stress [MPa]	Maximum strain [mm]
Ref.	-	-	*368,59*	*1189*	*0,01606*
1	0,2	9	327,46	982,7	0,01990
2		11	318,3	941,1	0,02514
3		13	309,15	927,4	0,03159
4		15	299,99	1090,0	0,03873
5		17	290,83	1165,0	0,03953
6	0,3	9	334,32	1018,0	0,01707
7		11	326,67	987,9	0,02038
8		13	319,02	950,5	0,02407
9		15	311,37	985,7	0,02791
10		17	303,72	1051,0	0,02767
11	0,4	9	340,79	1052,0	0,01541
12		11	334,68	1024,0	0,01737
13		13	328,37	996,1	0,01948
14		15	322,26	973,2	0,02158
15		17	315,95	1147,1	0,02092

The table data was plotted to better observe de parameter's influence on the results. With the graphical observation of the data it can be seen if the parameters present optimum values.

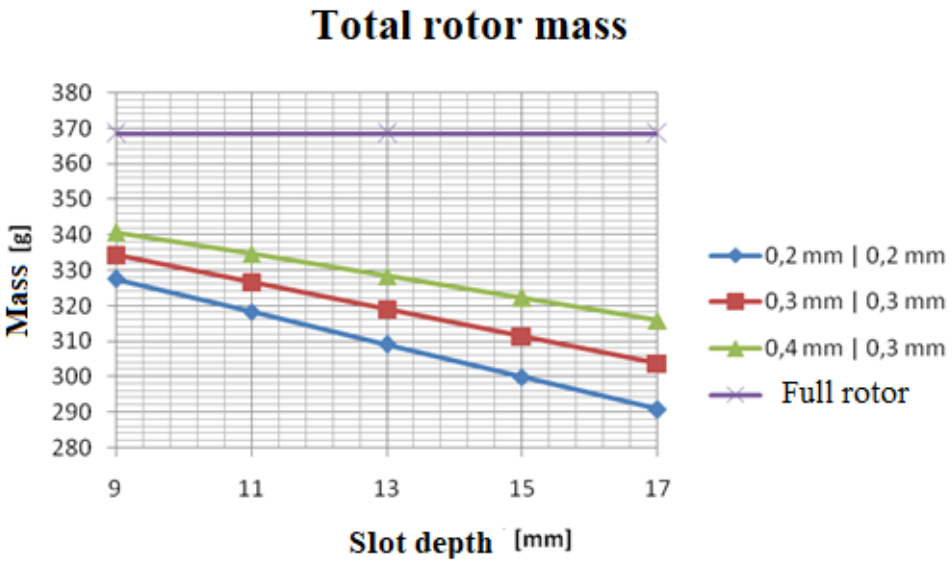

Fig. 3 Mass variation of studied cases

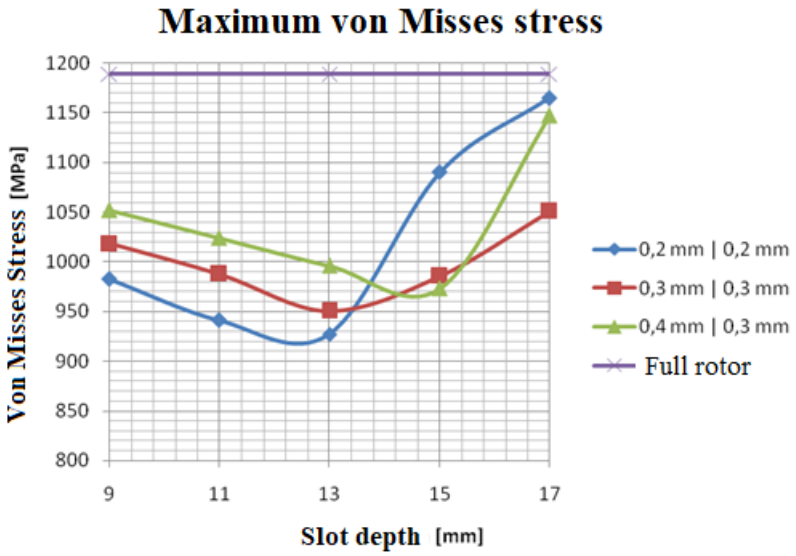

Fig. 4 Maximum stress variation of studied cases

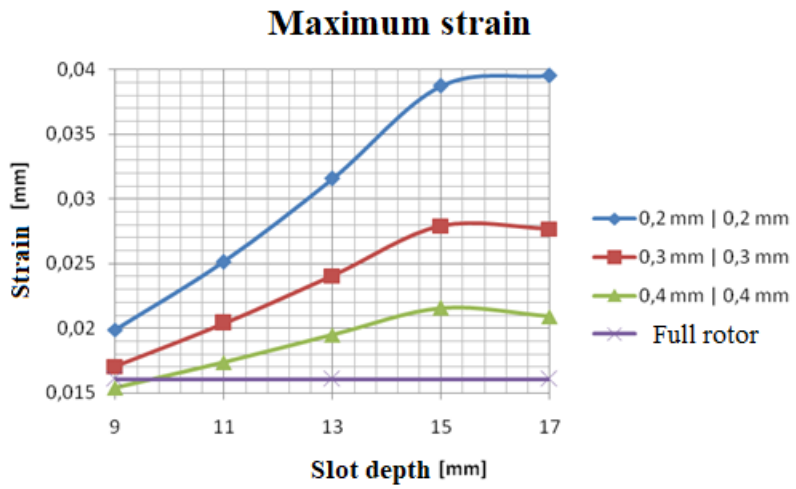

Fig. 5 Strain variation of studied cases

The Fig. 3 to 5 present the plots of the stress versus the slot depth for each case of wall thickness. There can be observed that for a given value of the wall thickness there is a minimum in stress and a maximum in strain. So, for the final rotor the values chosen for the rotor are:

- Wall thickness: 0.2 mm;
- Slot depth: 12.5 mm.

The reasoning behind this choice is that, from Fig. 4, we can see, that the chosen combination of wall thickness and slot depth offers the lowest von Misses stress. By seeing that this parameter offers an optimum value it was chosen as representative for the optimization. The mass does not present optimum values, as seen in Fig. 3, and neither does the value of strain, as seen in Fig. 5. That proved us that the aforementioned combination of values is the best for this case.

The calculations were realized with Solidworks 2018.

The boundary conditions were:

- Rotor is fixed by a frontal surface, a presumed shaft;
- The speed is 80000 rpm.

There are additional ribs created inside the rotor blade to ease the additive manufacturing process by giving the printed material a support on which the printer to build.

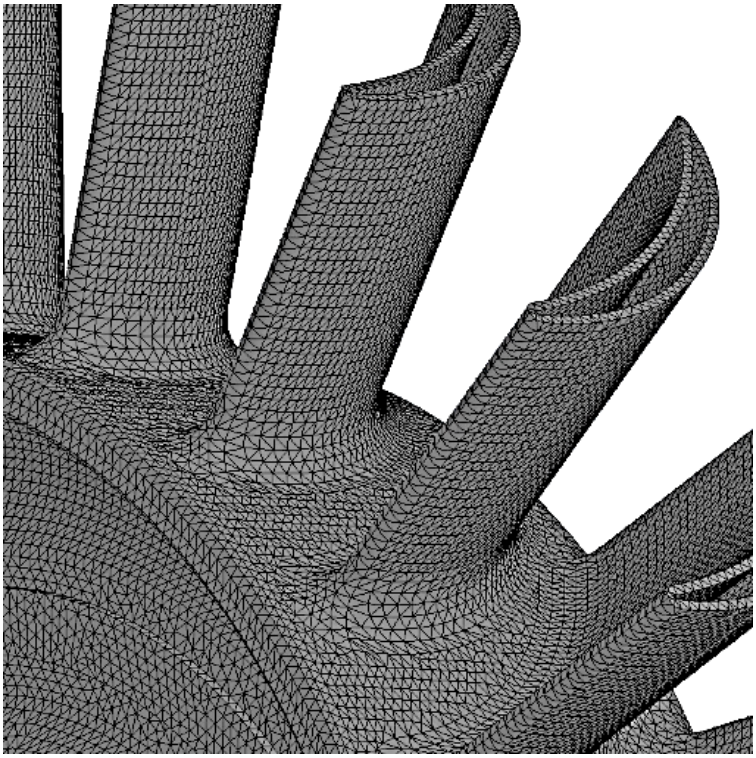

Fig. 6 The mesh used for the calculation

2.2. Dimensional tolerances of the rotor blade

With the blade design methodology completed, the next step is to set the part requirement for the 3D printing process. From the authors previous experience, we gathered a dimensional and surface quality requirement of the blade for the manufactured rotor. These requirements are, as seen in Fig. 3, maximum 0.15 mm material addition to the airfoil shape and a minimum distance between the blades also known as choke section with a tolerance of 0.02 mm.

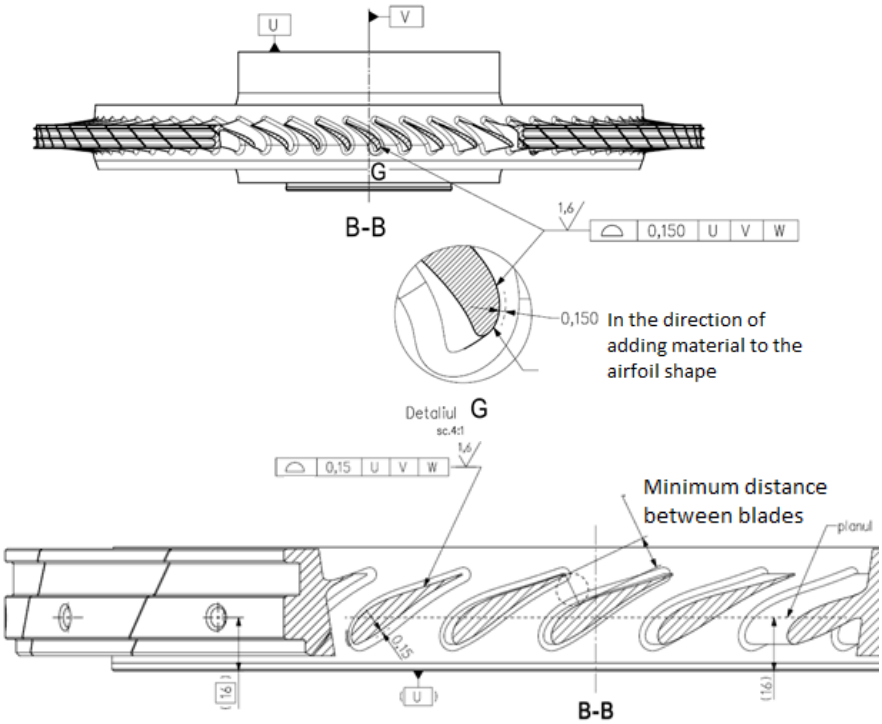

Fig. 7 The blade tolerances

Additional tolerances of the rotor are required like the shaft clearance and blade tip clearance. These types of dimensions that have precise tolerances must be taken into account when designing the rotor. If they exceed the 3D printer precision they must be limited and made machinable.

3. ADDITIVE MANUFACTURING CAPABILITIES

Now that the requirements of the turbine blade rotor are defined, the next step is studying the capabilities of the additive manufacturing technology in regards to the two defined requirements. For this task we created two ways of testing them.

3.1. Material strength of 3D printed metal

The stress of the printed material was tested using test samples situated at different angles on the printing table, and in different positions, to study a possible connection between orientation, position, and material strength. The test samples were manufactured in using the 3D printer EOS M270 and the material used was EOS – MP1 CoCr and machined according to SR EN ISO 6892-1. The choice in material, as opposed to section 1, was required because of different 3D printing machines with different

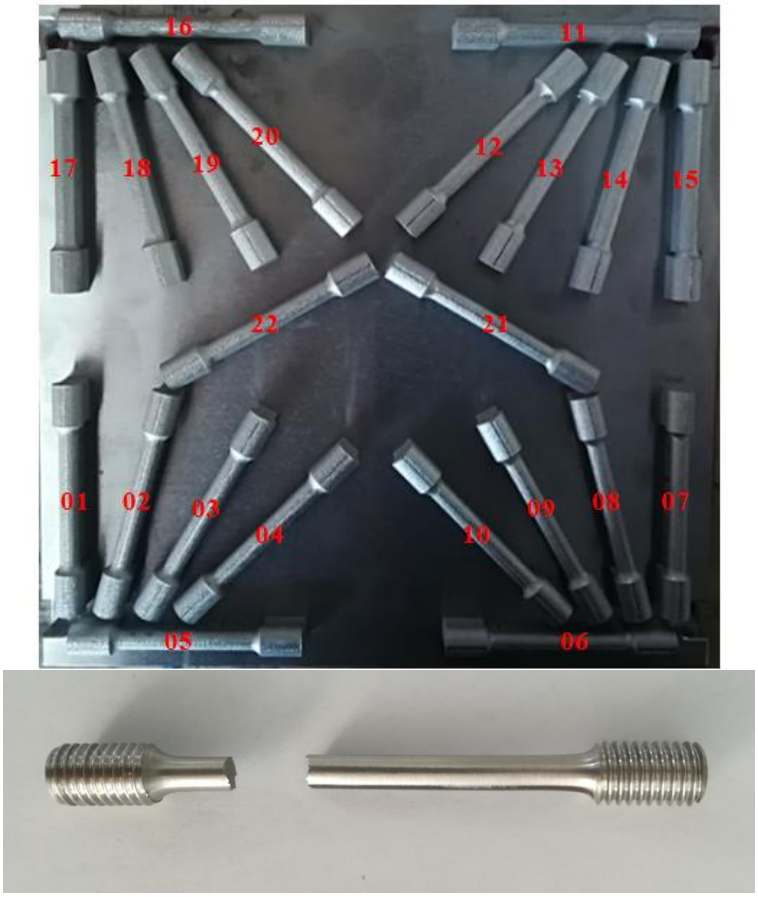

Fig. 8 The cylindrical rods on the table, used for manufacturing of the test samples, and the test sample after the test

The results were obtained by testing the samples using Universal Machine INSTRON 8802 (+/- 250 kN) fitted with an extensometer. In Fig. 9 the experimental test results regarding the mechanical properties of the test samples is displayed. The red lines represent the tensile stress recorded during the test in Fig. 9 a, and the load applied to the test subjects plotted against the time passed during the test in Fig. 9 b. The black dots represent the tensile yield strength and the ultimate tensile strength of the material.

a)

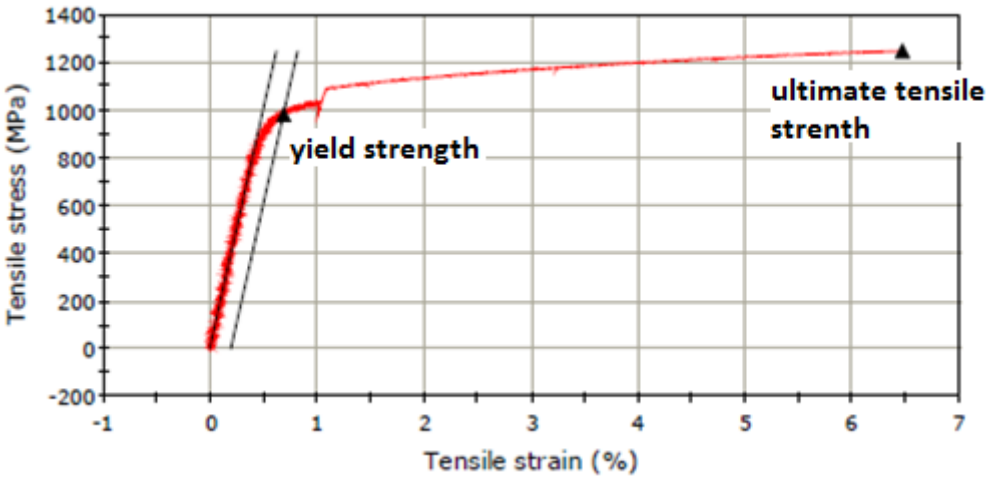

b)

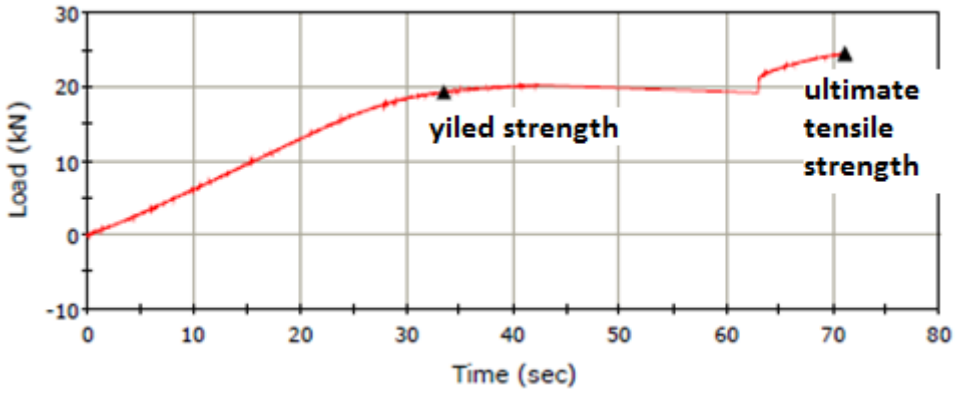

Fig. 9 The plotted data of the mechanical tests a) tensile stress vs strain b) load vs time

Table 2. Tensile tests results

No.	Temperature test [°C]	Ultimate load [kN]	Ultimate tensile stress [MPa]	Yield stress [MPa]	Strain [%]
1	Room temperature	31,02	1268,53	1000,38	9,5
2		28,82	1253,85	978,84	9,6
3		29,00	1252,45	994,19	9,9
4		-	-	-	-
5		29,01	1290,65	1007,51	10,6
6		24,21	1233,18	975,61	9,7
7		24,52	1248,97	990,08	9,7
8		24,93	1269,82	998,55	9,9
9		24,51	1248,52	984,19	8,3
10		24,32	1248,80	990,79	9,66

The ultimate tensile stress the maximum percentage difference is:

$$(1 - 1290,65/1233,18) \times 100 = 4,66\% \quad (1)$$

the yield stress difference is:

$$(1 - 1007,51/975,61) \times 100 = 3,26\ \% \quad (2)$$

and strain difference:

$$(1 - 10,6/8,3) \times 100 = 27,7\ \% \quad (3)$$

The differences are small and applicable in our rotor manufacturing.

3.2. Dimensional precision of 3D printers

For the study of the precision of the additive manufacturing machines, a different reference geometry of a blade rotor and stator row was selected. The blades were designed using [5] and printed using the EOS M270 machine. The printed geometry was scanned and compared to the CAD model for a dimensional analysis. The results are presented in Fig. 10.

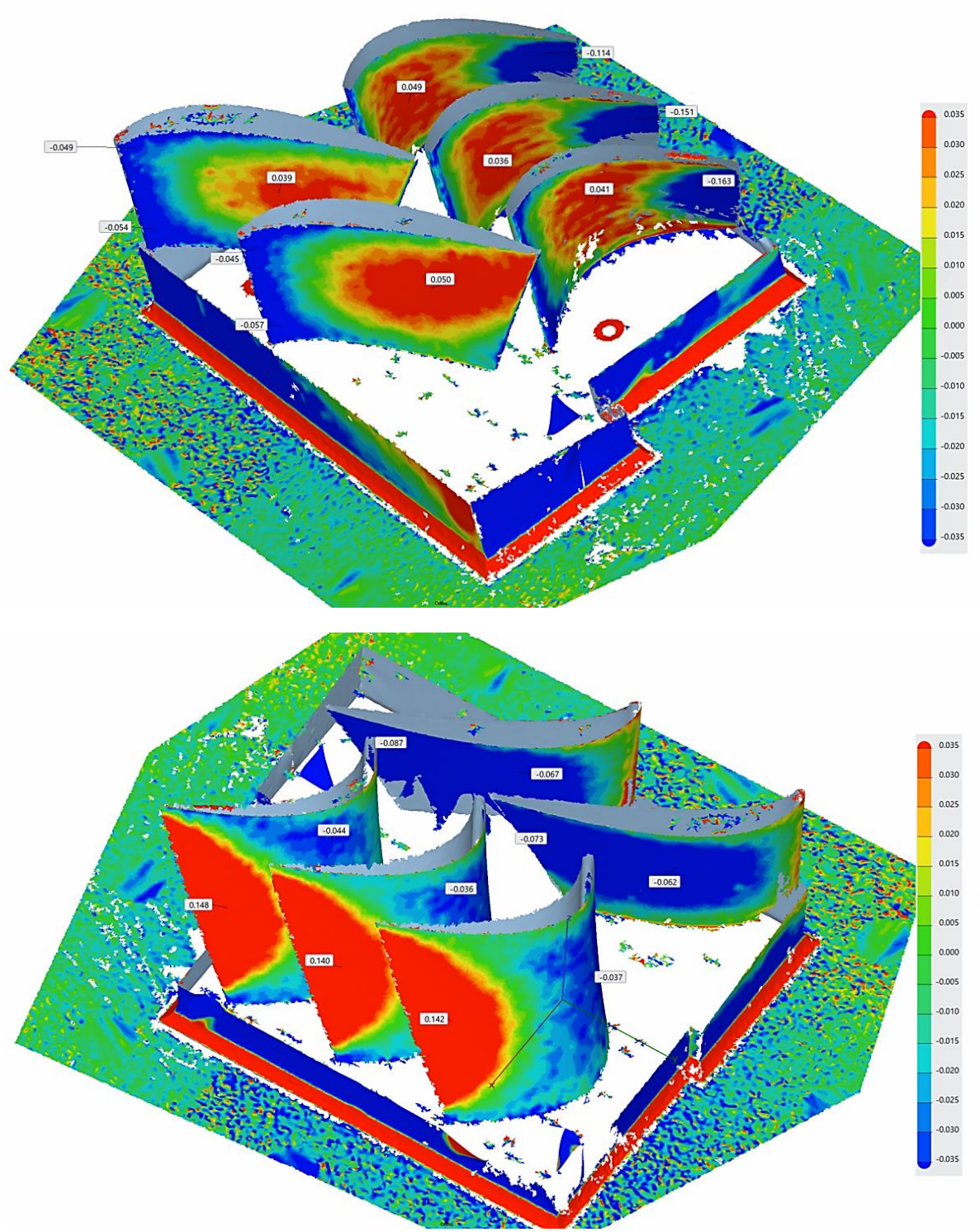

Fig. 10 Scan vs CAD model of the printed geometry

The green zones indicate a perfect match between the CAD and scanned model, the red zones indicate an addition of material and the blue zones indicate a lack of material. As can be seen the errors are situated between -0.163 mm and +0.148 mm and with the defined tolerances of ±0.15 mm and the fact that the red and blue zones are complementary on the blade, the shape is conserved so the results of the additive manufacturing process are acceptable

4. CONCLUSIONS

The paper defines the requirements usually found in liquid fuel rocket engine turbopumps and, using reference models of geometries, tested the capabilities of the additive manufacturing technology from the material strength and dimension precision standpoints. The results indicate that even in this initial form of the technology, it is fully capable of creating applications for the aerospace industry, differences being very small in terms of ultimate tensile stress, yield stress and strain, the values being 4.66%, 3.26% and 27.7% respectively, when compared to classical manufacturing process. Additional testing will be performed in different configurations of the rods on the printing table. The dimensional errors obtained for the additive manufacturing are between -0.163 mm and +0.148 mm, requirements being: ±0.15 mm.

This paper can be used for further research regarding the 3D printing technology application in the aerospace domain. More so, it can be used as a basis for implementation of the technology in a manufacturing process for a final product.

ACKNOWLEDGEMENT

The presented study was performed in the frame of 3dRotor project (Romanian Space Agency STAR Program, ctr. 138/2017) within COMOTI Romanian Research and Development Institute for Gas Turbines.

REFERENCES

[1] David Planchard, “SOLIDWORKS 2018 Tutorial with Video Instruction”, SDC Publications, 2018, ISBN 1630571563;
[2] ISO 6892-1:2016, International Organization for Standardization, 2016;
[3] “Instron Model 8802, 8803, 8804, 8805 and 8806 Load Frames Reference Manual - Pre-Installation”, Instron Corporation, 2001;
[4] "EOSINT M270 instruction manual", EN 1641 / EN ISO 22674, EOS company.
[5] C. Dobromirescu, V. Vilag, "Energy conversion and efficiency in turboshaft engines", SUSTAINABLE SOLUTIONS FOR ENERGY AND ENVIRONMENT (EENVIRO 2018), Conference: Cluj-Napoca, 2018, Book Series: E3S Web of Conferences, Volume: 85, Article Number: 01001, DOI: 10.1051/e3sconf/20198501001;

In its third year, Space Tech Expo Europe is the continent's major dedicated supply-chain and engineering event for manufacturing, design, test and engineering services for spacecraft, subsystems and space-qualified components. The exhibition and free-to-attend conference draw attendance from thousands of industry leaders, decision makers, engineers, specifiers and buyers to meet manufacturers across the supply chain for civil, military and commercial space.

New for 2019: Space Tech Expo Europe launched an exhibition and conference dedicated to this fast-growing sector of the space industry.

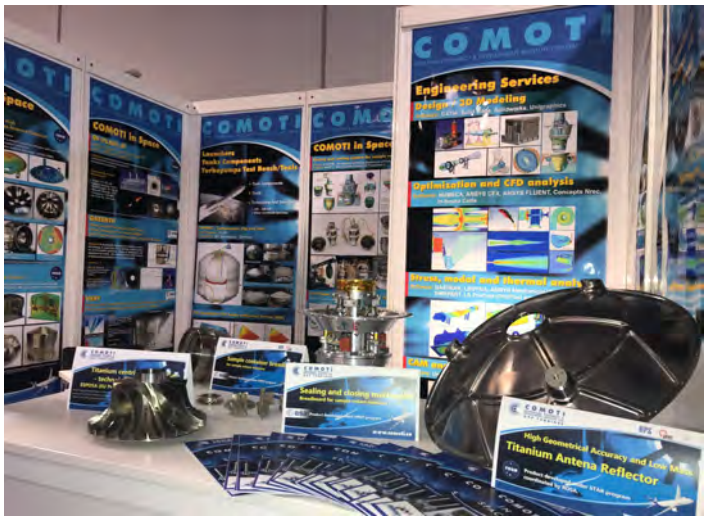

COMOTI

The only specialized company that integrates such activities as

scientific research,
design,
manufacturing,
testing,
experimental activities,
technologic transfer and innovation

in the field of aircraft and industrial gas turbines and high speed bladed machinery.

220D Iuliu Maniu Ave., 061206 Bucharest, ROMANIA,
P.O. 76, P.O.B. 174
Phone: (+4)021/434.01.98, (+4)021/434.02.31, (+4)021/434.02.40
Fax: (+4)021/434.02.41, e-mail: contact@comoti.ro

www.comoti.ro